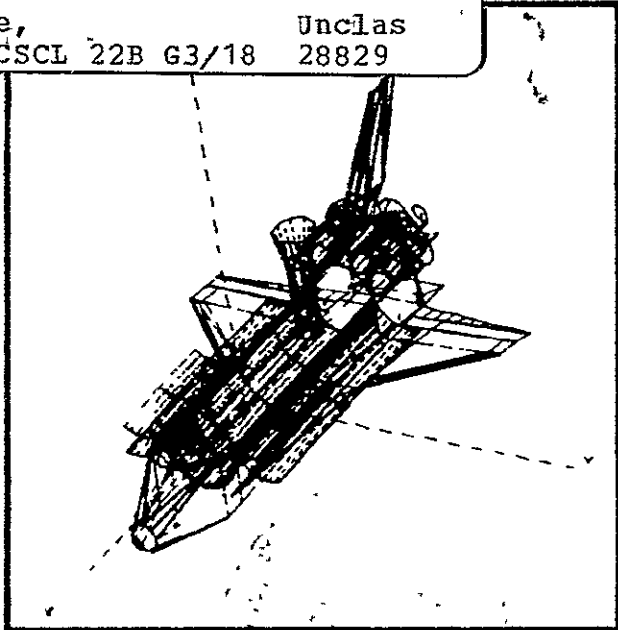MCR-78-578
NAS2-9816

CR-152171

Final
Report

August 1978

Experimental Investigation of Contamination and Contamination Prevention Techniques to Cryogenic Surfaces On Board Orbiting Spacecraft

(NASA-CR-152171) EXPERIMENTAL INVESTIGATION OF CONTAMINATION PREVENTION TECHNIQUES TO CRYOGENIC SURFACES ON BOARD ORBITING SPACECRAFT (Martin Marietta Aerospace, Denver, Colo.) 96 p HC A05/MF A01 CSCL 22B

N78-29146

Unclas
G3/18 28829

MARTIN MARIETTA

EXPERIMENTAL INVESTIGATION OF CONTAMINATION AND
CONTAMINATION PREVENTION TECHNIQUES TO CRYOGENIC
SURFACES ON BOARD ORBITING SPACECRAFT

By

M. A. Hetrick, R. O. Rantanen, E. B. Ress and J. F. Froechtenigt

August 1978

Distribution of this report is provided in the interest of
information exchange. Responsibility for the contents re-
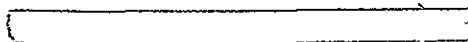sides in the authors or organization that prepared it.

FOREWORD

This report is submitted in accordance with Article V,
paragraph A.a.3 of Contract NAS2-9816. NASA technical monitors
for this study were John Vorreiter and Constantine Pappas, NASA-
AMES, Moffett Field, California.

TABLE OF CONTENTS

TABLE OF CONTENTS (Cont.)

1.0 INTRODUCTION

1.0 INTRODUCTION

1.1 _Purpose_ – The purpose of this study was to experimentally investigate the feasibility of using gaseous helium as a purge to actively prevent contaminant gases from reaching cryogenic surfaces of an infrared telescope system while on-orbit. An earlier analytical study by Murakami[1] indicated that to effectively drive condensible molecules from such a telescope, helium pressures in the 10^{-6} Torr range would be required.

Therefore, the goal of this study was to determine experimentally the helium pressures and flow rates required to significantly reduce the incoming flux of contaminant molecules under simulated orbital conditions using a scale model telescope and relating these measurements to a full scale system such as the Shuttle Infrared Telescope Facility (SIRTF). The contaminant gases of concern to SIRTF are ambient atmospheric species (primarily atomic oxygen) and water from the Shuttle Orbiter surfaces and flash evaporator (see Witteborn and Young[2] and Simpson and Witteborn[3]). The source of helium for the purge could be an augmentation of the primary supply of liquid helium used in cryogenically cooling the telescope optical components. By reducing the flux levels of the contaminants, the on-orbit degradation of critical operational surfaces by these contaminants would be minimized and the operational activities and lifetime of the telescope would be significantly increased.

1.2 _Approach_ – The approach taken during this feasibility study was to simulate the orbital velocity (energy) of the contaminant species by accelerating ions of N_2, O and H_2O gases with an ion gun. The interaction of the gases within an infrared telescope was simulated by constructing a one-tenth scale telescope assembly. The telescope model was patterned after the full scale SIRTF facility shown in Figure 1-1 (see Reference 4). For this feasibility study, the optical components inside the telescope were not simulated. Only the telescope barrel, sunshade and plane of the primary optics were fabricated. The contaminant gases were accelerated as ions and detected as a current on the various sections of the telescope. A mass spectrometer located in the plane of the primary mirror monitored the ions and neutrals reaching the bottom of the telescope. Helium was injected as a purge gas at the bottom end of the telescope from both a small porous disc and a nozzle. The reduction of the incoming contaminant gases was then monitored as a function of helium purge pressure, helium purge gas temperature and incident ion energy.

1-1
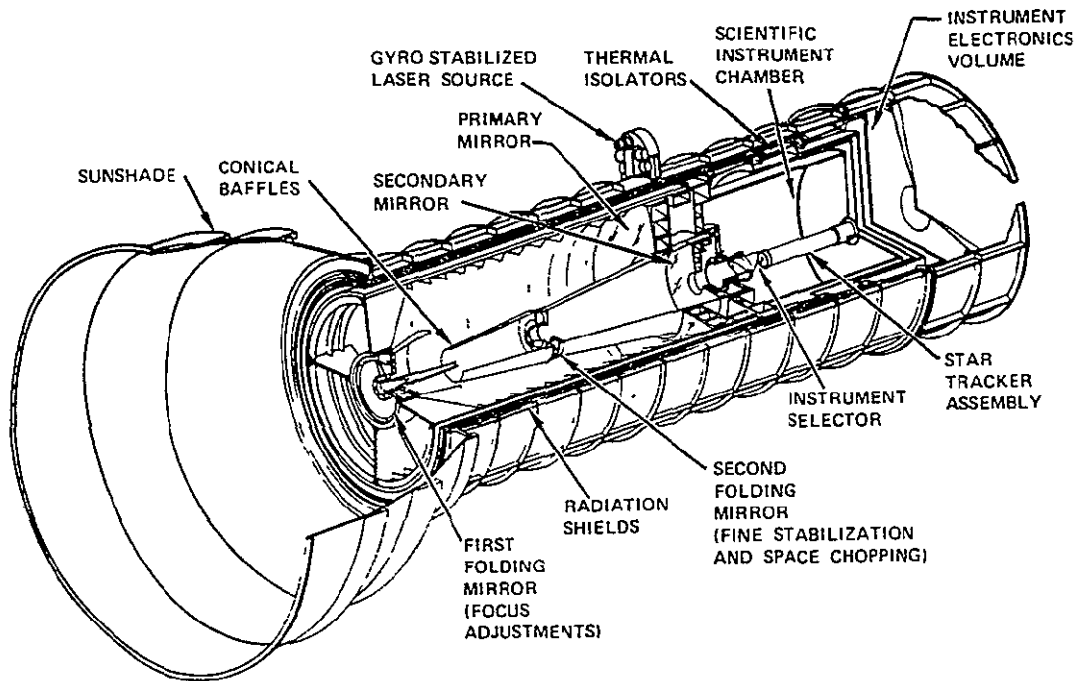
Figure 1-1 SIRTF Telescope (Taken from Reference 4)

The first phase of testing utilized N_2^+, O^+ and H_2O^+ ions and a diffuse helium injector. The second phase evaluated the use of a high expansion ratio nozzle as a helium source. The third phase determined if neutral contaminant species could be detected by introducing nitrogen gas into the test volume as a charge exchange medium.

A beam of high velocity contaminant ions were used in the test rather than a neutral beam for the following reasons:

a) this study was exploratory in scope with the purpose of determining the feasibility of a helium purge concept,

b) helium/ion collision cross sections were not expected to be significantly different from He/neutral cross sections,

c) a thermal source of 5-10ev neutrals required impractical temperatures (10^4K), and

d) an ion beam could be generated with relative ease while neutralizing the beam would require considerable sophistication to the experimental instrumentation.

1.3 <u>Summary</u> – A one-tenth scaled model of the SIRTF basic configuration was constructed for testing in the Space Physics Laboratory at Martin Marietta Denver Division. The on-orbit ambient contaminant environment was simulated in the laboratory's 1.2x5.2m vacuum chamber with an ion beam kit. Details of the test chamber, ion source, telescope model and instrumentation are discussed in Section 2.0. Helium was injected into the model telescope at the simulated plane of the primary optics. Two helium injection techniques were investigated, a) porous plug, and b) nozzle. More details are provided in Section 2.4. The purge gas and telescope components were cooled to 140K in several cases to ascertain the effect of gas temperature.

Ion flux at the simulated plane of the primary optics was monitored with an electrometer and a mass spectrometer as discussed in Section 2.5.

Scaling criteria were developed in Section 3.0 to translate the model data to the full scale configuration.

Table I-1 summarizes the significant test conditions that are discussed in Section 4.0. Ion beam attenuation for N_2^+, O^+, H_2O^+ and O_2^+ has been plotted as a function of the model telescope pressure.

Significant conclusions drawn are:

- Within the limitations of this simulation of on-orbit conditions, it was demonstrated that a helium purge system can be an effective method of reducing the incoming flux of contaminant species.

- A helium purge system would appear to be a feasible technique for reducing deposition of condensibles on cryogenic surfaces and for extending the operational lifetime of the SIRTF.

- Experimental telescope pressures required for 90% attenuation appears to be slightly higher than predicted by Murakami (1).

- The use of a 25 degree half-angle nozzle to inject the helium was slightly less effective than a porous plug. An optimum nozzle may not have been employed.

Table 1-I   Test Condition Summary

Run Number	Contaminant Gas	Energy (eV)	Velocity (km/s)	Stopping Medium	Gas Temp(K)	Type Injection
168	N_2	9.0	7.8	Helium	300	CHS
169	N_2	15.0	10.0	Helium	300	CHS
172	N_2	50.0	18.7	Helium	300	CHS
154	N_2	59.5	20.5	Air	300	CHS
181	N_2	10.8	8.7	Helium	140	CHS
182	N_2	10.8	8.7	Helium	140	CHS
183	N_2	10.8	8.7	Helium	300	Nozzle
184	N_2	10.8	8.7	Helium	300	Nozzle
164	O	4.5	7.4	Helium	300	CHS
163	O	7.0	8.7	Helium	300	CHS
156	O	24.7	17.1	Air	300	CHS
155	O	34.7	21.0	Air	300	CHS
166	H_2O	5.4	7.6	Helium	300	CHS
167	H_2O	9.4	10.0	Helium	300	CHS
185	H_2O	8.0	9.2	Helium	300	Nozzle
186	H_2O	8.0	9.2	N_2	300	Nozzle
187	H_2O	8.0	9.2	N_2	140	Nozzle
173	N_2	50.0	18.7	Helium	140	CHS
159	O_2	19.0	10.8	Helium	300	CHS

1.4 Nomenclature

A	ampere
cm	centimeter
eV	electron volt
g	gram
K	degrees Kelvin
KN	Knudsen number
L	characteritic length
l	path length
m	meter
$\dot{m}$	mass flux
mm	millimeter
$\overline{N}$	average number density
N_a	Avagadro's number
N^a	molecular density
NCD	number column density
P	Pressure
R	Universal gas constant
r_o	radius of telescope aperture
s	second
T	temperature
v	velocity
λ	mean free path
μ	micron
ρ	density
σ	cross section

SUBSCRIPTS

f_s	full scale
m	model
o	aperture

2.0 TEST CONFIGURATION

2.0   TEST CONFIGURATION

This study was conducted in the Space Physics Laboratory at Martin Marietta Aerospace, Denver Division using the laboratory's main test chamber. The overall test configuration is shown schematically in Figure 2-1. The separation distance from the exit of the ion source to the base plate of the scale telescope was 1.5 meters. Figure 2-2 is a photograph of the scale model telescope integrated into the vacuum chamber. Figure 2-3 shows the RGA and ion gun power supplies. As shown, the main power supplies for the ion gun were isolated and enclosed since they float at high potentials above ground. A more detailed discussion of the major test components is contained below. A list of instrumentation is contained in Appendix A.

2.1   Test Chamber – The main test chamber in the Space Physics Laboratory is made of stainless steel and is 5.2 meters long and 1.2 meters in diameter. Access to the chamber is through a 1.2 meter hinged end cap which allows quick access to the experimental setup. The pumping system consists of a 0.928 liters/s roughing pump and a 0.41 meter oil diffusion pump. A liquid nitrogen cold trap is situated above the diffusion pump to eliminate any backstreaming of oil into the test chamber. The normal operating pressure for the test chamber with no gas injection is in the 10^{-6} Torr range. Pumpdown time for the chamber is approximately 1.5 hours.

An initial evaluation was made on the helium pumping capability of the chamber by pumping down to approximately 10^{-6} Torr and then bleeding helium into the chamber. The helium flowrate was increased until the pressure in the chamber had stabilized at around 10^{-3} Torr. The valve between the diffusion pump and chamber was then closed with the helium still flowing into the chamber. The pressure increased rapidly and the valve to the diffusion pump was then reopened as indicated in Figure 2-4.

Based on the pressure rise rate in the chamber, a helium flowrate of approximately $1x10^{-2}$ g/s was calculated to be entering the chamber. It was concluded that at a chamber pressure of $1x10^{-3}$ Torr the pump could handle $5x10^{-3}$ g/s or about 20 times
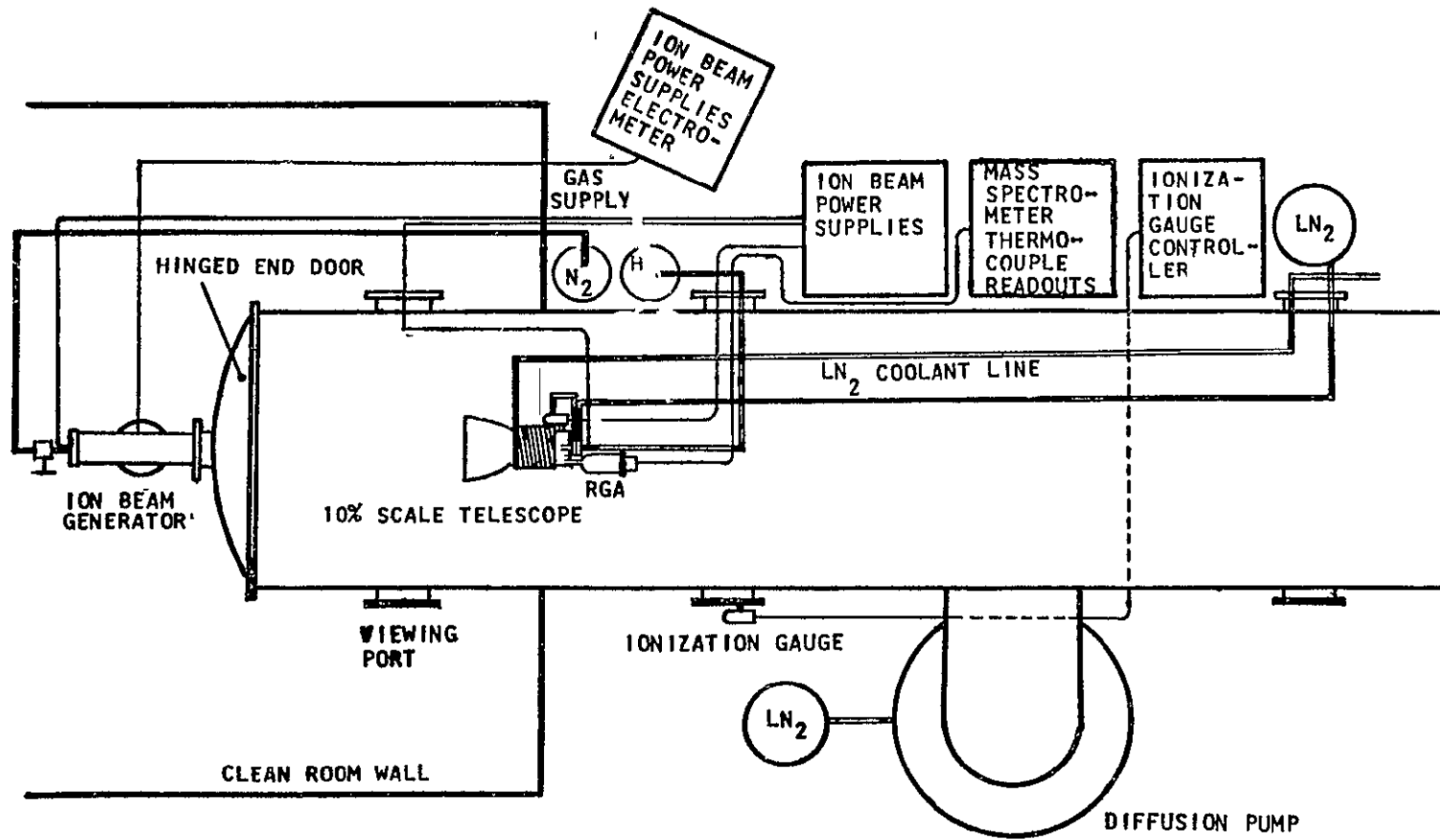
Figure 2-1 Test Schematic for Helium Purge Feasibility Study
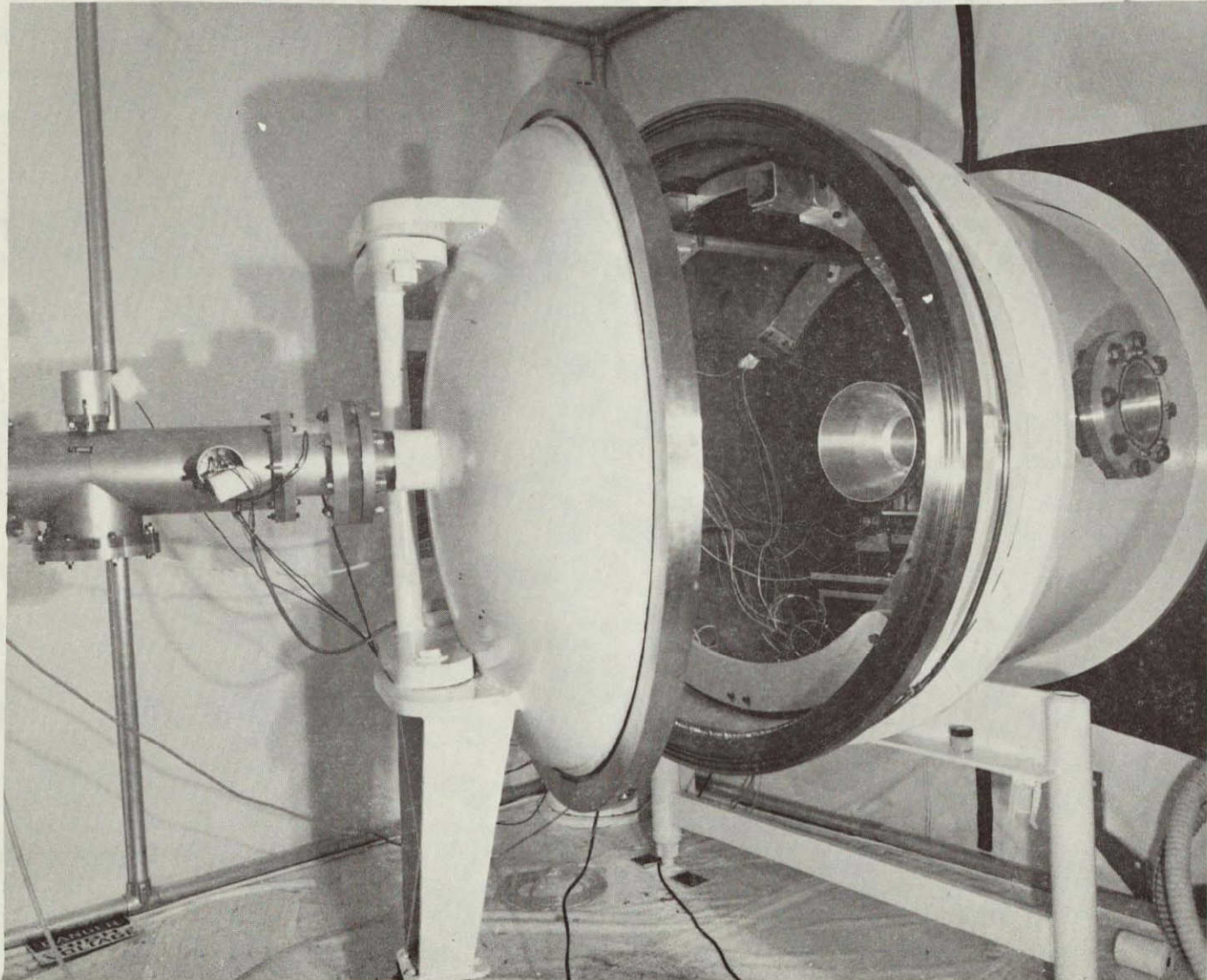
Figure 2-2a   Test Configuraton Showing Major Components
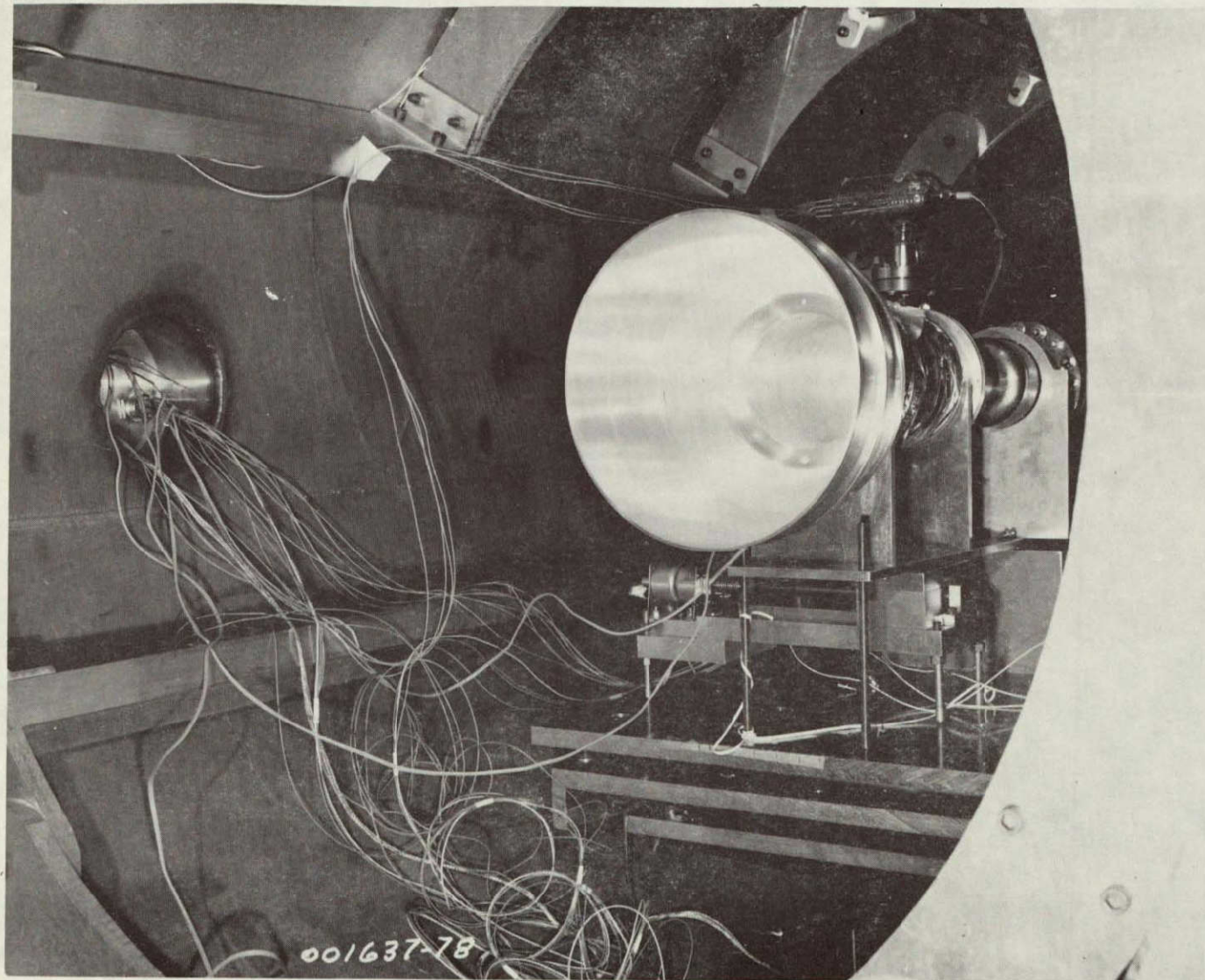
Figure 2-2b   Test Configuration Showing Major Components
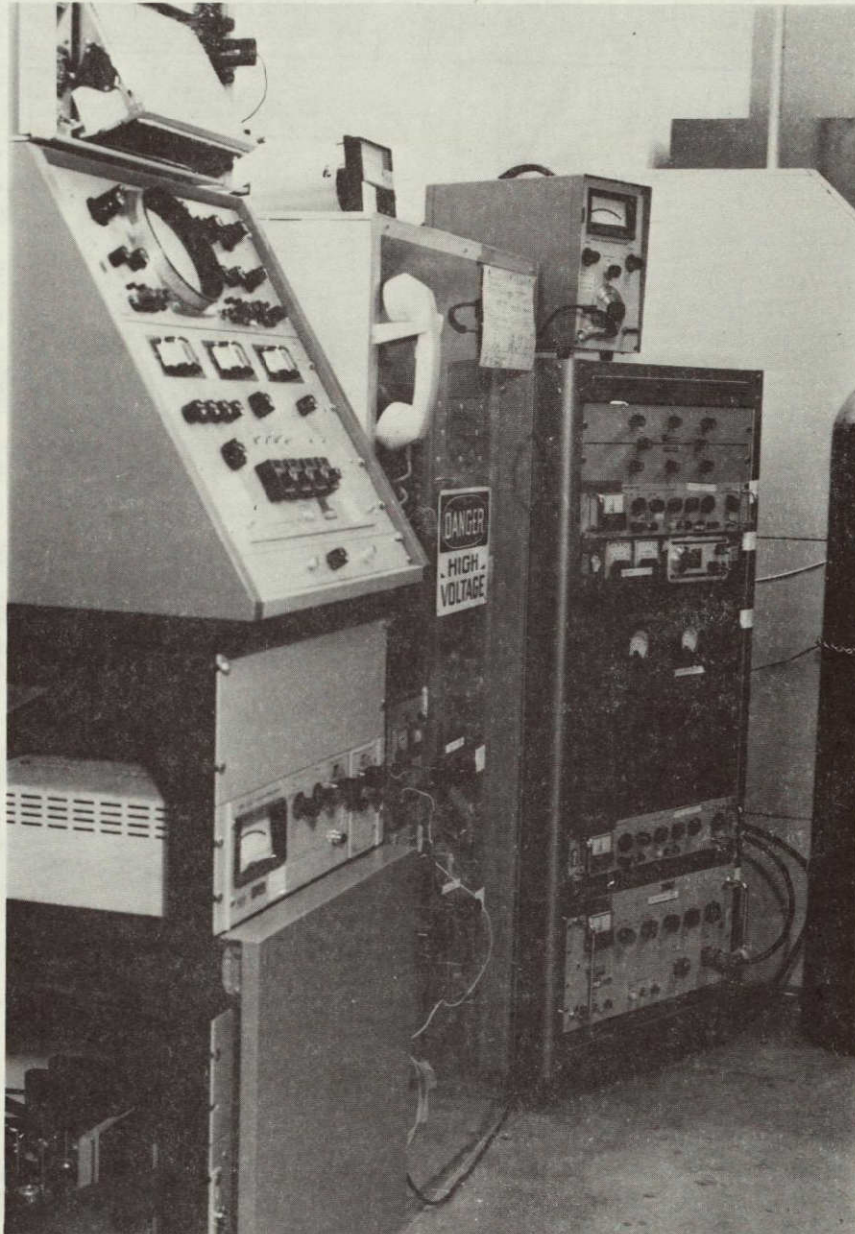
Figure 2-3   RGA and Ion Gun Power Supplies

$$\frac{dp}{dt} = \frac{9.5 \times 10^{-4}}{.8} \times 6 \quad \text{(FACTOR FOR HELIUM)}$$

$$= 7 \times 10^{-3} \text{ Torr/s}$$

1.0×10^{-4} Torr (N_2 EQUIVALENT)

PUMP ON

PUMP OFF

1 s

0.9
0.8
0.7
0.6
0.5
0.4
0.3
0.2
0.1
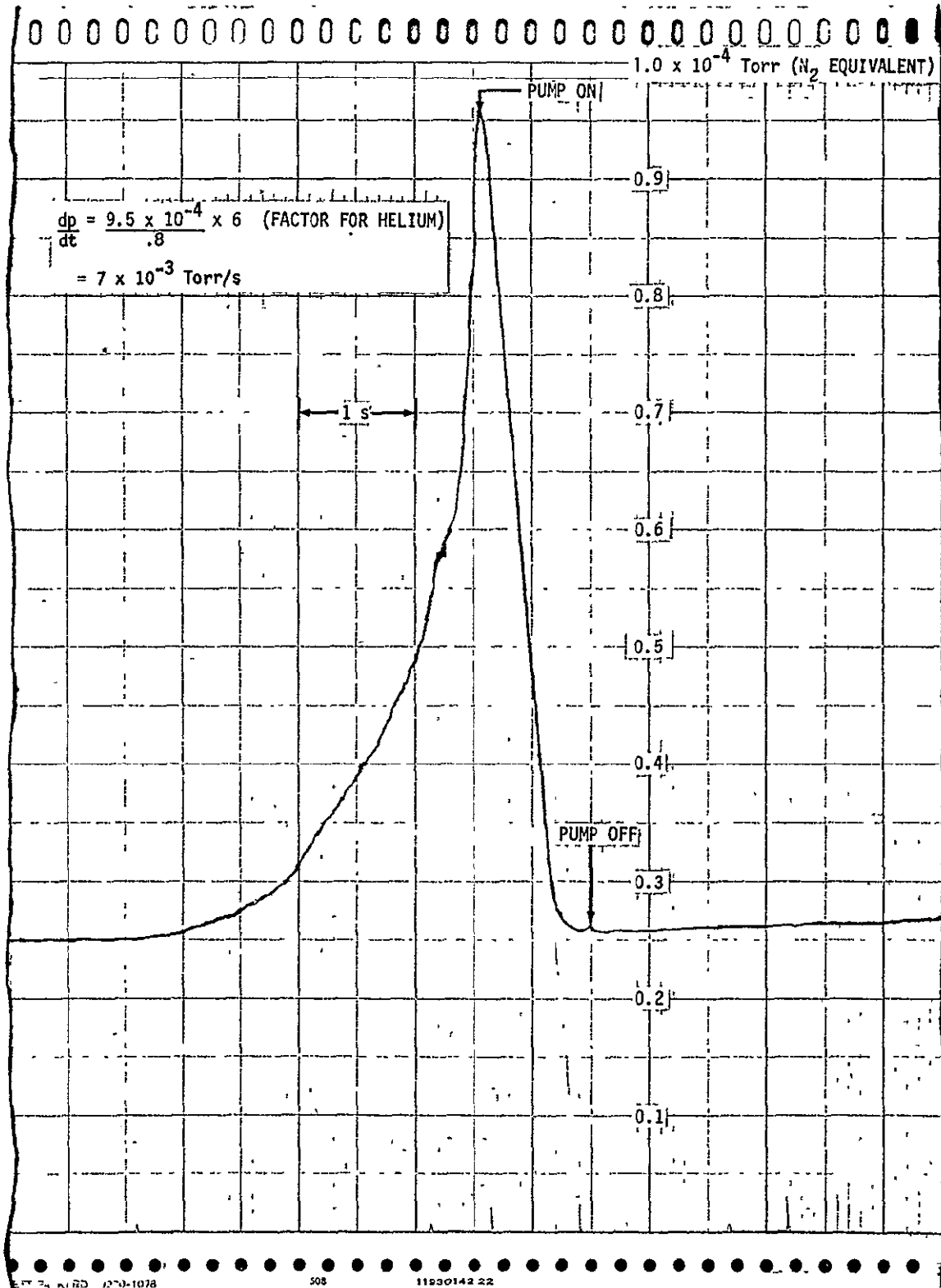
Figure 2-4   Chamber Pressure History With Helium Flow

the rates anticipated for the one-tenth scale model telescope
purge. When the pump was again on-line, the chamber pressure
dropped to near original value within 2 seconds. Also as part
of the checkout, the helium purge was discontinued and the dif-
fusion pump was taken off-line. The chamber pressure was moni-
tored and an effective leak rate of approximately 10^{-5} g/s was
computed from the pressure rise rate.

2.2 <u>Ion Beam Gun</u> – An Ion Beam Kit model G-1 from Colutron
Corporation, Boulder, Colorado was used as the source of ions
for the test and, as shown in Figure 2-5, it was mounted on the
end flange of the vacuum chamber. The Colutron Ion Beam Kit
consists of an ion source, heat sink, acceleration and focus-
ing system, vertical deflection plates, velocity filter,
velocity filter guard ring control unit and decelerator.
Figure 2-6 is an exploded drawing of the major elements of the
ion beam gun. Figure 2-7 is an electrical schematic of the ion
beam gun.

The ion beam gun can be operated from approximately 5eV to
over 5keV with ion currents of a few microamperes. The velocity
filter analyzer can supply mass separated beams with a resolu-
tion of up to M/ΔM=200, where ΔM is the full width at half
peak height. The dispersion of the mass separated beam is ad-
justable. The energy spread of the ion beams produced by the
ion beam gun has been measured to be as low as 0.11eV. The
overall length of the gun when assembled is approximately 0.41
meters.

Sources of O_2 and N_2 for the ion gun were obtained from
standard laboratory K bottle gas supplies. The H_2O source was
obtained by assembling a canister which could be sealed and
valved to a small roughing pump and then metered into the ion
gun as indicated schematically in Figure 2-8. The roughing
pump was used to remove dissolved gases from the water prior to
bleeding into the ion gun. In order to establish a 100 μ
pressure at the ion source, the water in the canister was
heated to generate sufficient water vapor pressure to support
the ion gun.

The procedure for operating the ion gun was to first
activate the 20 mil filament by slowly applying a 20A current
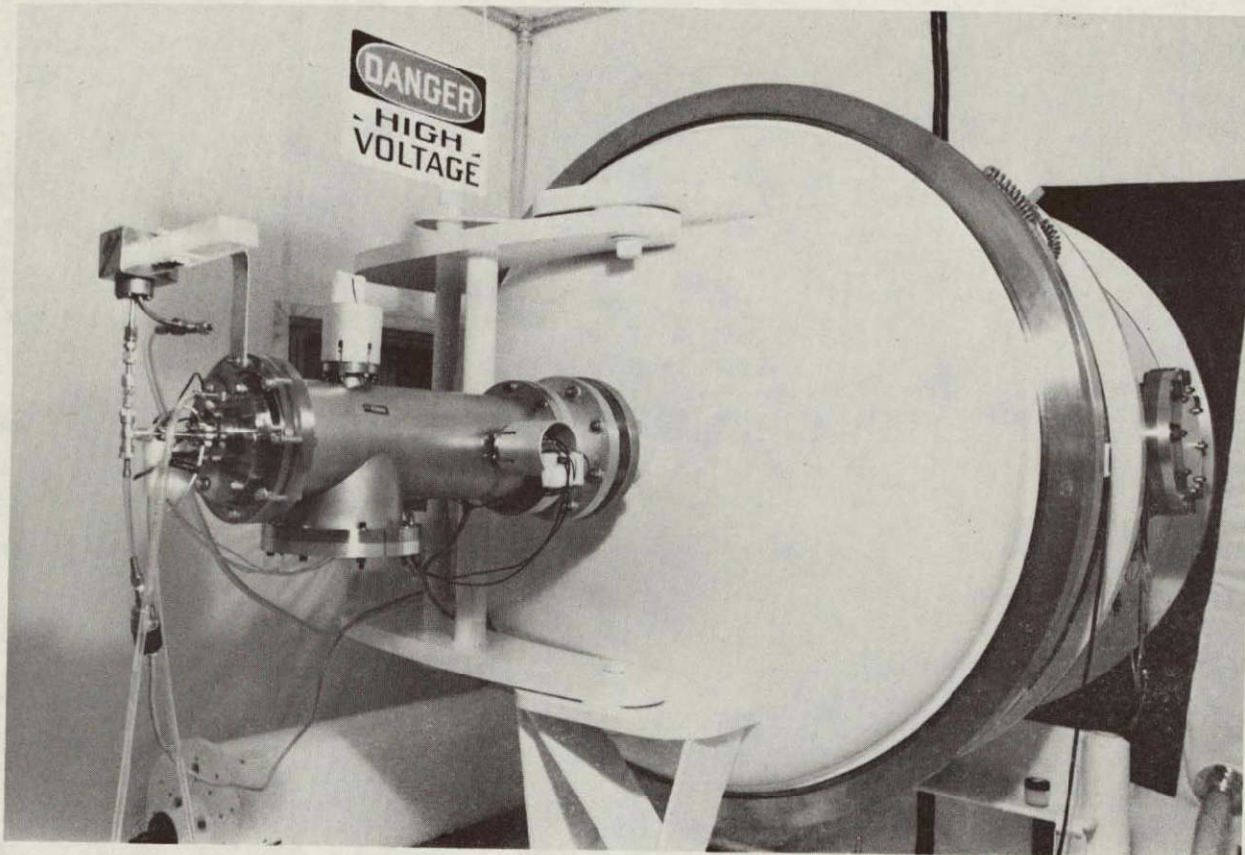
Figure 2-5   Ion Gun Mounted on Test Chamber

DECELERATOR

VELOCITY FILTER

ION SOURCE RECEPTACLE

HEAT SINK

VERTICAL DEFLECTION PLATES

ACCELERATION AND FOCUSING SYSTEM

GAS INPUT

SOLID CHARGE INPUT

PLUG-IN ION SOURCE
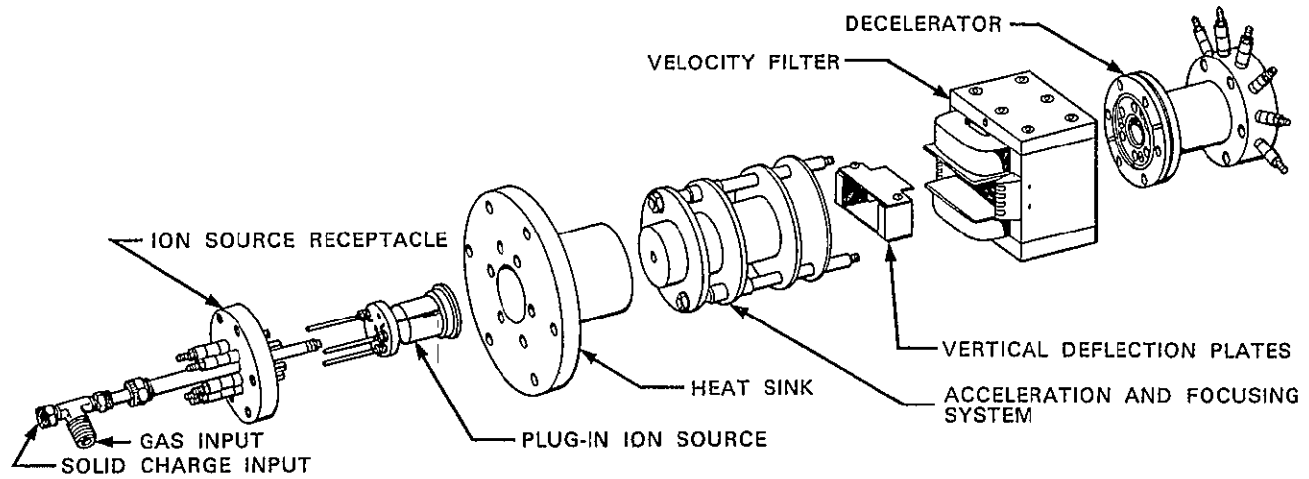
Figure 2-6 Exploded View of the Major Elements of the Ion Beam Gun
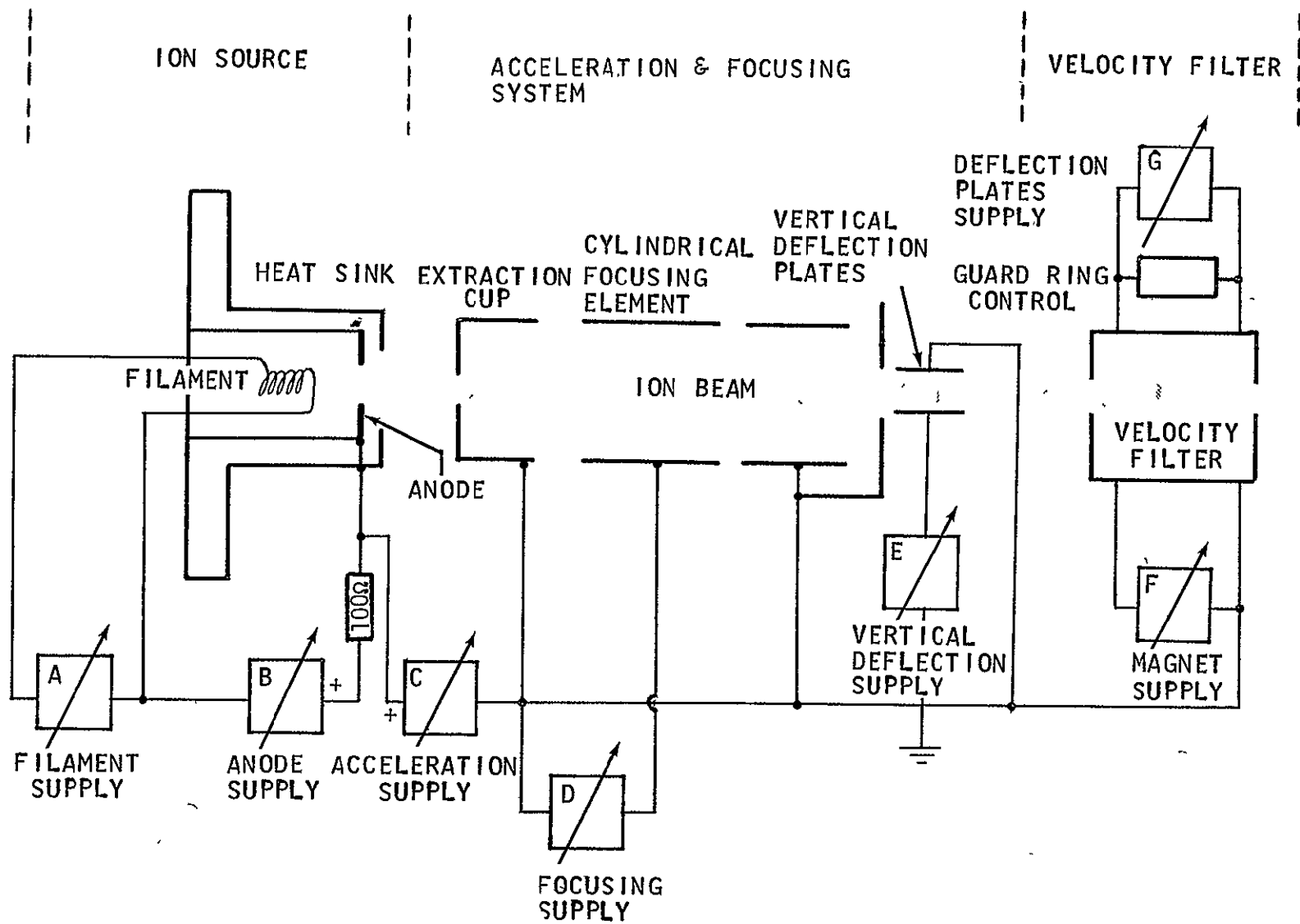
Figure 2-7 Electrical Schematic of Ion Beam Gun
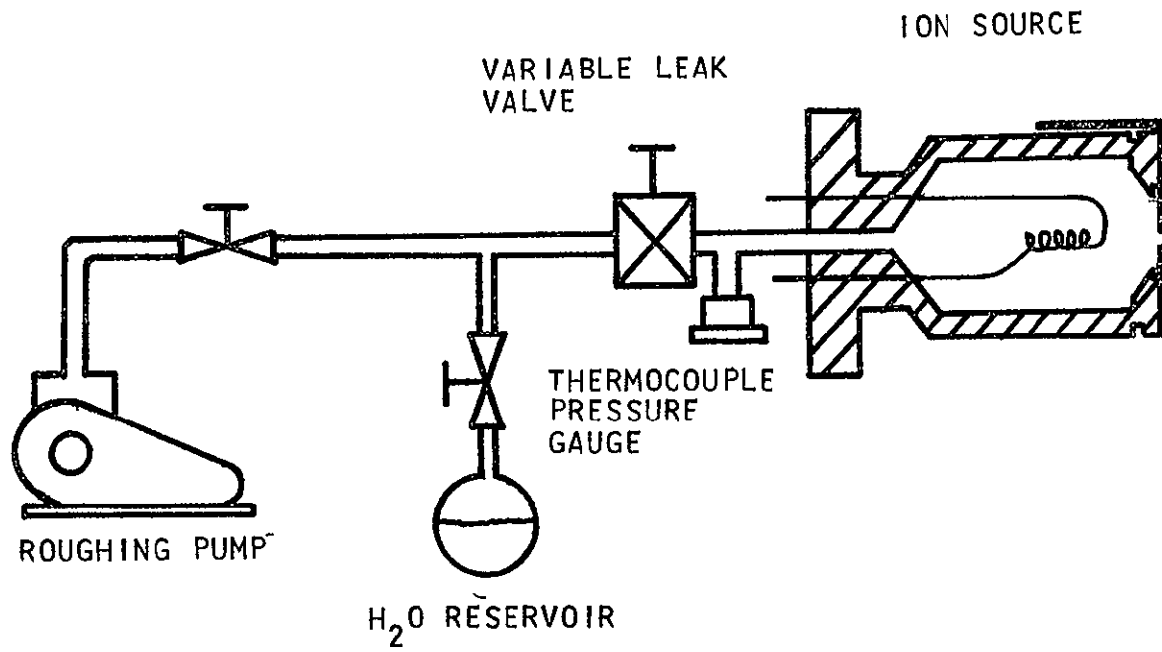
Figure 2-8   Schematic for Water Vapor Source

with power supply A (see Figure 2-7). It takes approximately
10 to 15 minutes to outgas the filament when operating the ion
gun after the chamber has been open to ambient. Next, a poten-
tial of 150 volts is created between the filament and the anode
with power supply B. A Granville-Phillips variable leak valve
is then slowly opened to allow the gas into the ionization
chamber. When the inlet pressure increases to around 100 μ ,
an arc initiates through the gas as indicated by an instantane-
ous current surge of approximately 1 A on power supply B. (A light
purple glow discharge characteristic of nitrogen can be seen in
the ionization chamber by viewing through the plexiglass end
flange on the ion gun.) The anode current is then reduced to
around 0.2 to 0.5A for normal operation.

An accelerating voltage of 10 volts (for a 10 eV beam) is
then applied between the anode and ground (when the target is
at ground) with power supply C. The fourth power supply that
is activated (supply D) maintains the first cylindrical focus-
ing element at about 2/3 the acceleration voltage. Power
supply E is used for fine tuning the position of the beam.

The velocity filter consists of a magnet powered by supply
F and a pair of electrostatic deflection plates (supply B)
mounted to produce an electric field perpendicular to the mag-
netic B field. The mass number that passes through the filter
undeflected is a function of the applied $\mathcal{E}$ and B·fields as
shown below:

$$M = 2e \cdot V \cdot \left(\frac{B}{\mathcal{E}} \right)^2 \tag{2-1}$$

where e = 1.60×10^{-19} coulombs,
   V = acceleration voltage,
   B = magnetic field strength and
   $\mathcal{E}$ = applied electric field strength (V/m).

The strong focusing effect normally associated with this
type of filter (Wien Filter) has been overcome in the Colutron
filter by shaping the $\mathcal{E}$ and B fields with biased guard rings
and tapered magnet pole plates. A more detailed discussion
of the velocity filter in the Colutron ion gun is provided by

Wahlin[5]. Figure 2-9 illustrates the interrelationship between the velocity filter voltage and magnetic field strength to select a particular ion with a desired velocity. Given a gas such as N_2, the ion source generates both N_2^+ and N^+ ions. The velocity filter then separates out the N_2^+ ions from N^+ ions.

Ion beam mapping data for beam uniformity was acquired for several beam velocities and detection geometries prior to inserting the telescope assembly into the chamber. For example, a 12 cm x 12 cm brass plate was placed 1 meter in front of the ion gun. A Keithley 610A electrometer was used to measure the ion current intercepted by the plate. The front surface of the plate was painted with zinc sulfide which fluoresced under bombardment of the ion beam. A 200 eV beam of N_2^+ and N^+ ions produced a current of 1×10^{-4} A and a fluorescent spot about 3 cm in diameter. At 10 eV, the current collected by the plate was around 2×10^{-8} A with no discernable glow.

In another series of tests, a 0.64 mm diameter wire 15 cm long was traversed across the beam using the mechanism designed to translate the telescope assembly. Stepping motors with digital readouts were used to move the mechanism across its 15 cm of travel. 200 steps were equivalent to about 2.5 cm (8 steps/mm). Without attempting to focus the beam, the diameter of a 500 eV beam was measured to be around 6-7 cm in diameter with the ion flux dropping off 3 orders of magnitude at the edge over a 1.5 cm distance as shown in Figure 2-10. A similar test for a 20 eV beam indicated a beam with relatively uniform flux over the entire sweep of the traversing mechanism.

An estimate of the divergence or spreading of the beam was made by observing the amount of current collected on the sunshade of the model telescope versus the amount collected on the baffle section and end plate simulating the primary optics. On run 146, for example, where the aperture of the telescope was 1.0 meters from the ion gun, a current of 0.5×10^{-9} A was collected by the tube or baffle section of the telescope. The ratio of effective acceptance angle viewed from the ion source for the three telescope sections are listed in Table 2-I.
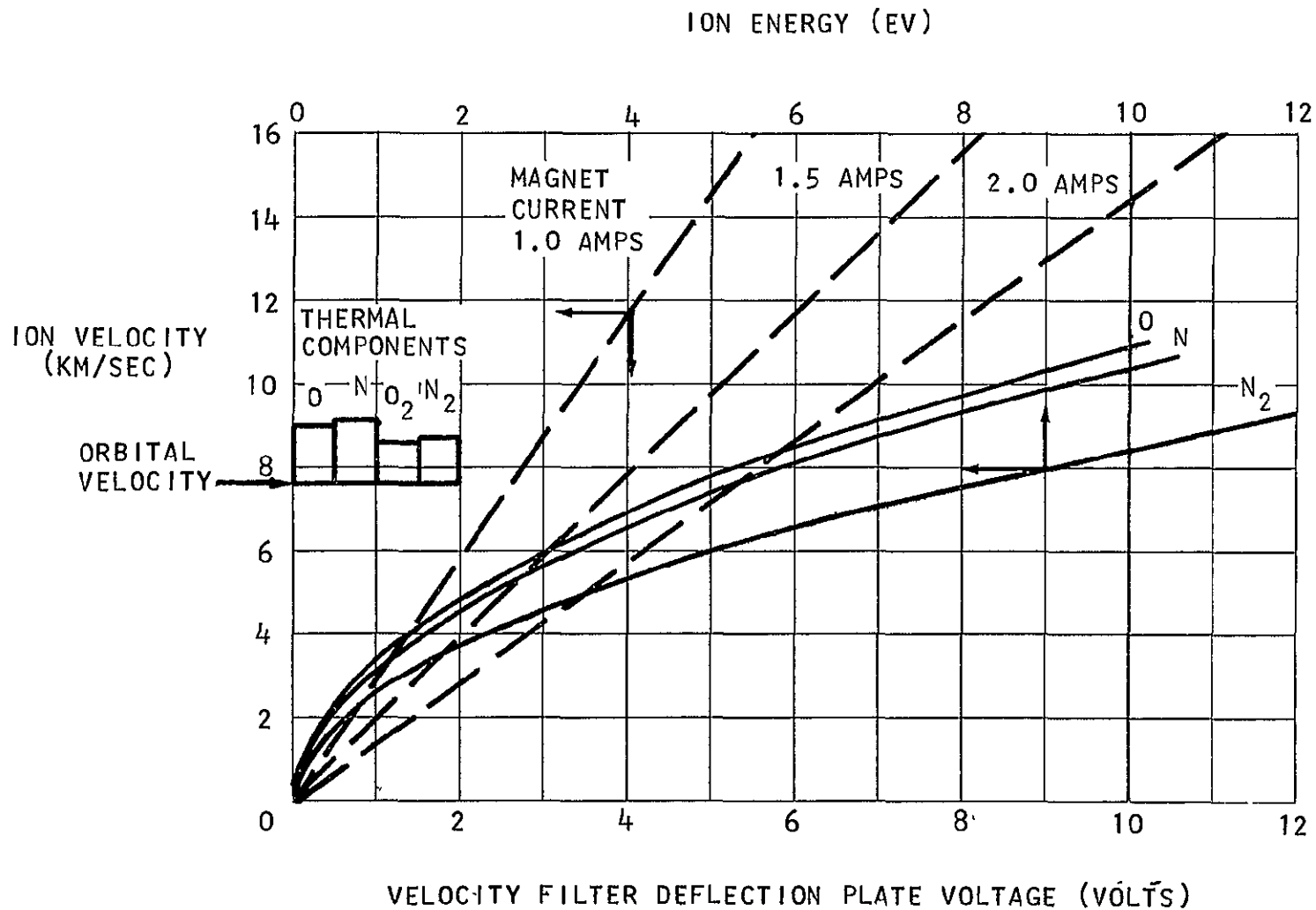
Figure 2-9 Velocity Filter Voltage and Magnet Current Settings to Select Specific Ions

GEOMETRIC
CENTER LINE

500 EV N_2^+ AND N^+ IONS

N_2 INLET PRESSURE = 100 μ

COLLECTOR: 0.64MM X 15CM WIRE

WIRE CURRENT (A)

10^{-8}

10^{-9}

10^{-10}

LATERAL DISTANCE (CM)
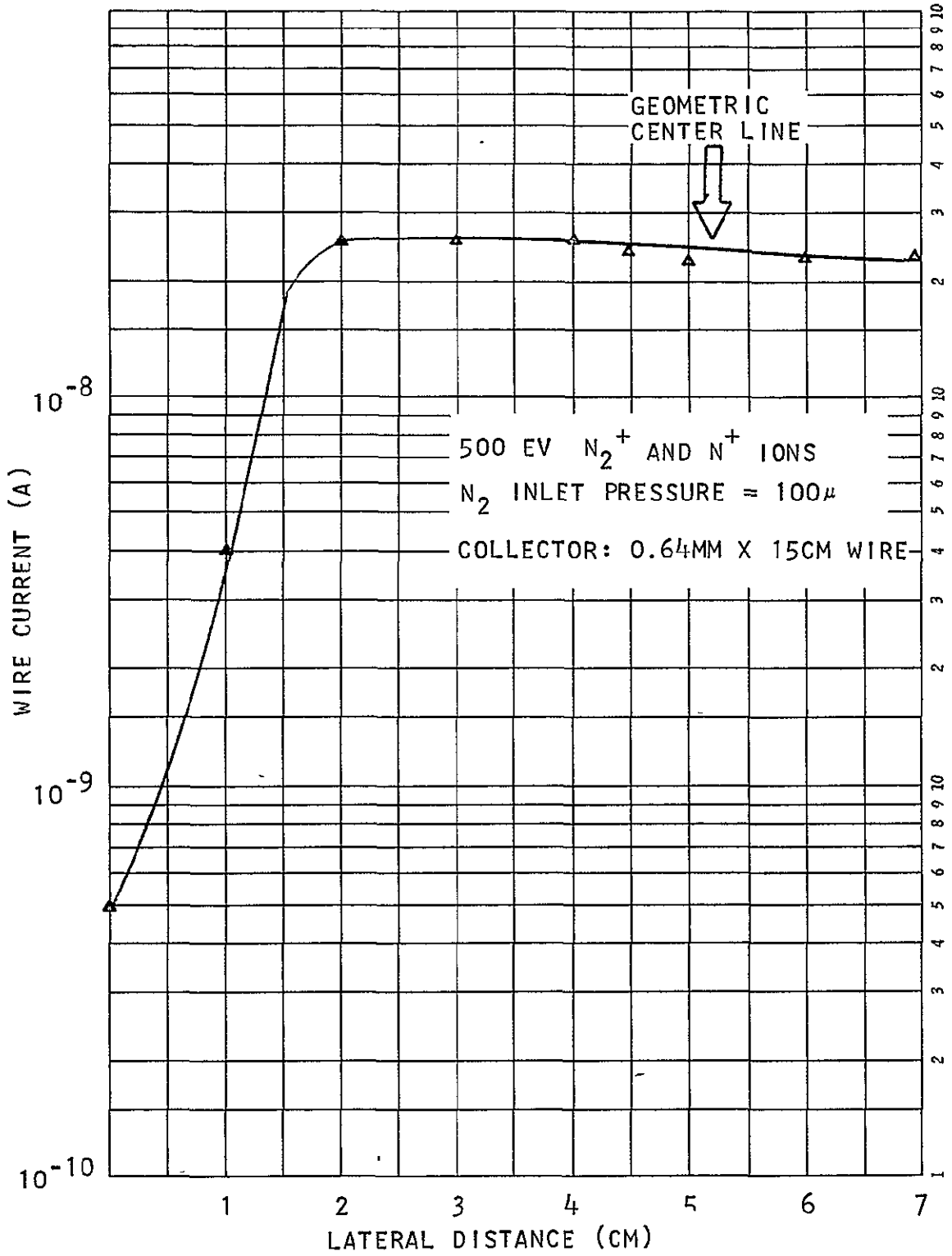
Figure 2-10   Beam profile Measured with Wire

Table 2-I   Ion Currents to Modeled Telescope Components

Section	I (A)	Acceptance Angle (Degrees)	Solid Angle	Current Flux (A/steradian)
Primary Optics	0.5×10^{-9}	0 to 2.45	0.00574	87×10^{-9}
Baffles	0.04×10^{-9}	2.45 to 3.0	0.00287	14×10^{-9}
Sunshade	1.5×10^{-9}	3.0 to 8.2	0.05563	27×10^{-9}

Although the peak current flux is impinging on the end plate, there is indication that the baffle section and sunshade were seeing some direct flux. The ions incident on the sunshade could either be the primary beam of N_2^+ ions which have diverged beyond 3 degrees or from the N^+ beam which was deflected laterally by the velocity filter. In any case, there is reason to believe the beam intensity at the end plate has decreased by nearly two orders of magnitude due to a 2 to 3 degree divergence.

2.3 Telescope Configuration – To simulate an infrared telescope system, a one-tenth scale model of the SIRTF configuration with the sunshade in a deployed configuration was constructed, as shown in Figure 2-11, with the ionization gage, RGA insulator block, and the helium gas inlet assembly used for the diffuse injector. Figure 2-12 illustrates the dimensions of the configuration and the location of the RGA and ionization gage. Engineering drawings of the overall telescope and test related instrumentation setup, sunshade design and telescope housing are provided in Appendix B. Each of the major components of the telescope and associated test instrumentation were designed so that they could be electrically isolated. This allowed the current to any component of the telescope to be measured independently.

2.4 Helium Purge Gas Injection System – For this feasibility study, a generalized helium injection technique was investigated which utilized a source of purge gas located at the center of the telescope in the plane of the primary optics. Two methods of injecting the helium were evaluated. These were a porous plug type injector (i.e., collimated hole structure) and a convergent/divergent high expansion ratio nozzle. The reason for using the convergent/divergent nozzle concept was
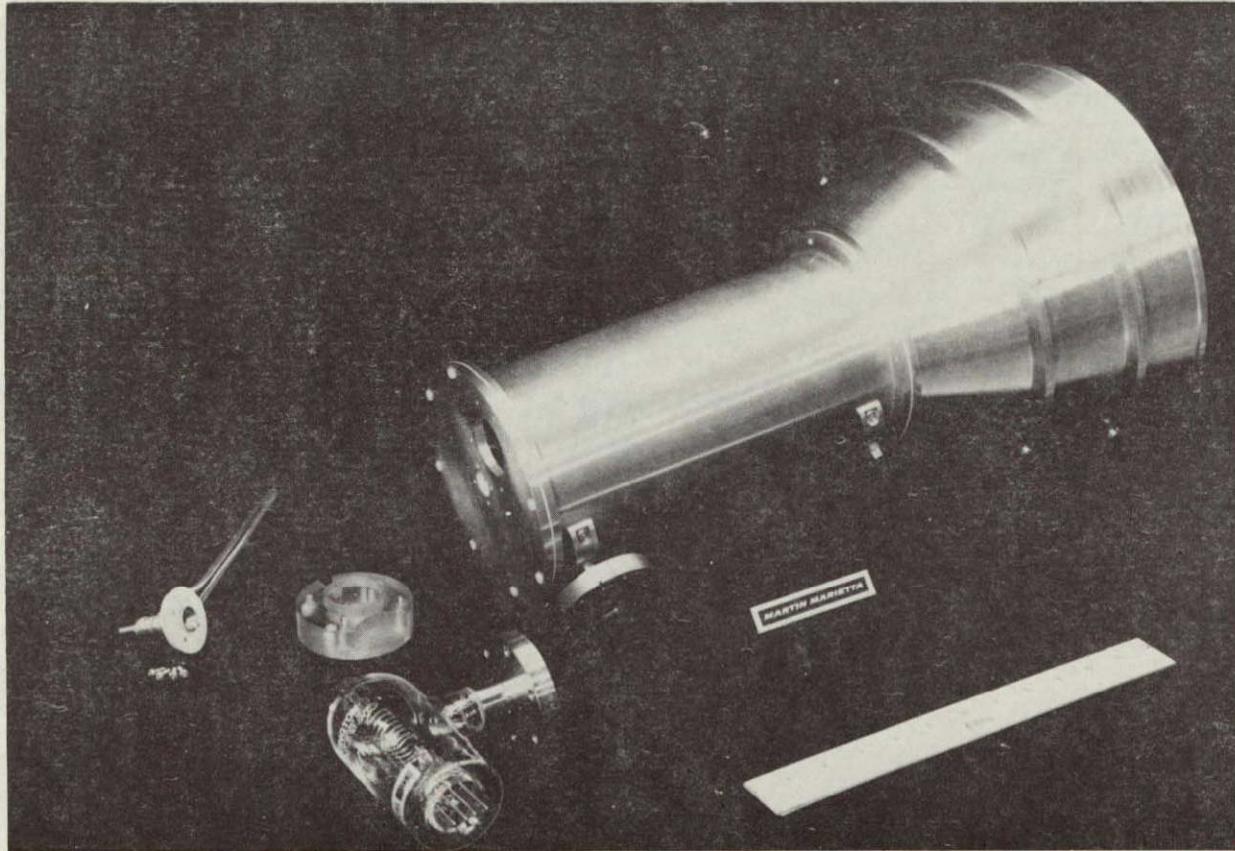
Figure 2-11 Picture of One-Tenth Scale Model Telescope Assembly
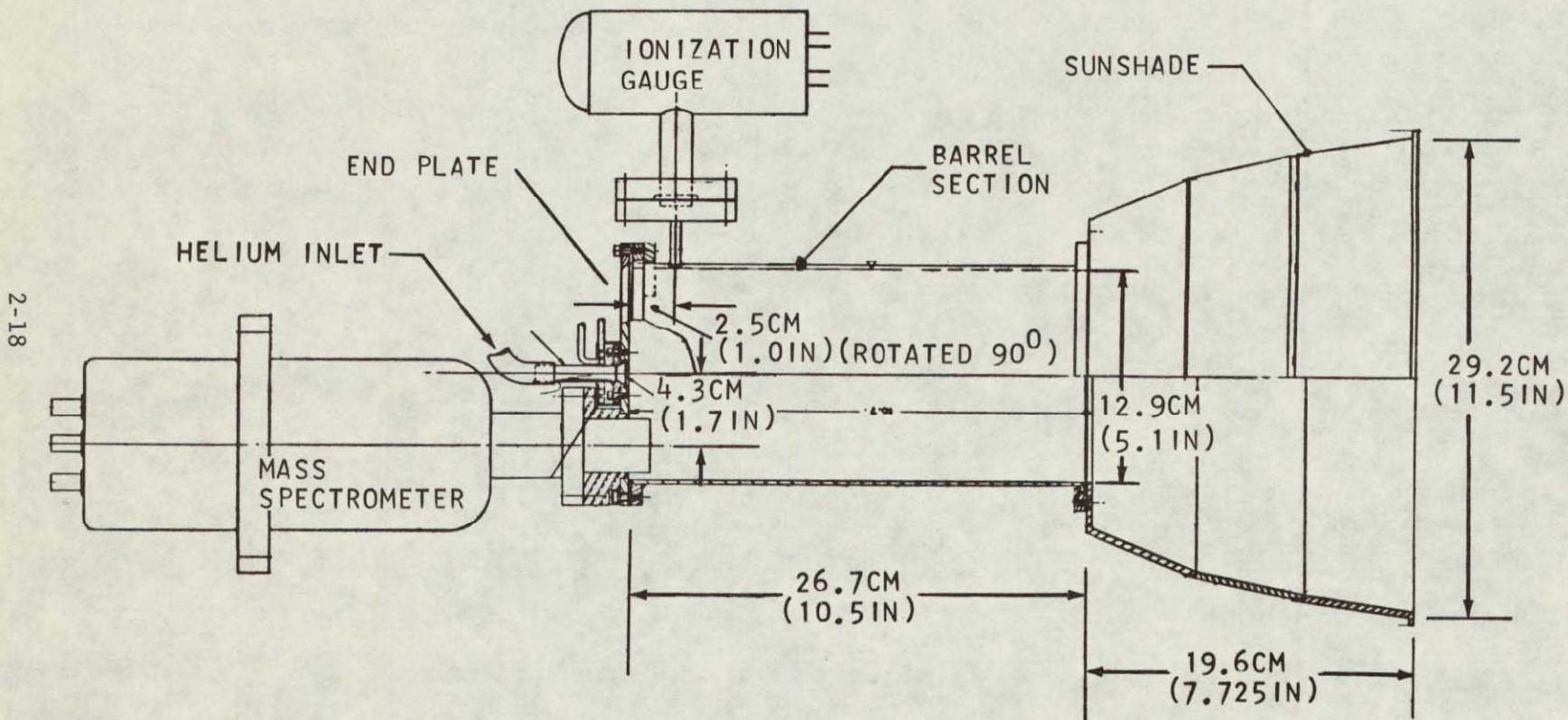
Figure 2-12   Telescope Configuration Illustrating the Location of the RGA and Ionization Gage

to convert a significant portion of the random motion of the
helium into directed or axial motion. Although the nozzle con-
cept should enhance the effectiveness of a given mass flow of
helium purge gas, it is a continuum flow device and its appli-
cability for this particular application which utilizes low
pressures was questionable.

2.4.1 Porous Plug Injector - A Brunswick Corporation colli-
mated hole structure (CHS) inlet grid system was employed as
the diffuse source. Figure 2-13 is a photograph of the CHS
grid structure magnified 65 times. The CHS is a porous metal
structure containing a controlled number and distribution of
discrete parallel capillaries. This inlet grid was 1.6 cm in
diameter and contained 335,000 holes 1.27×10^{-3} cm in diameter.
The CHS is made from stainless steel and its capillaries have
an aspect ratio (l/d), nominally, of 40.

2.4.2 Convergent/Divergent High Expansion Nozzle - The
convergent/divergent high expansion nozzle was designed using
inhouse computer programs. One of the problems in designing
such a nozzle is to bridge the gap between continuum nozzle
flow and free molecular conductances situations. Vacuum tech-
nology suggests that flow from a capillary tube with a length
to diameter ratio of 10 to 20 will be collimated. Continuum
nozzle expansion theory indicates high Mach number nozzles con-
centrate the mass flow in the free plume about the nozzle
centerline. However, as the flow becomes rarefied in the
nozzle, the continuum expansion concepts become invalid and
free molecular concepts must be used.

There are several considerations in designing a hypersonic
nozzle for acceptable flow. Although it appears desirable to
aim for a uniform (i.e., constant Mach number and zero angu-
larity) flow at the exit, this is nearly impossible to achieve.
For this particular application, the situation is further com-
plicated by the low operating pressures which result in low
operating pressures which result in low Reynolds numbers (i.e.,
the viscous forces become comparable to inertial forces).
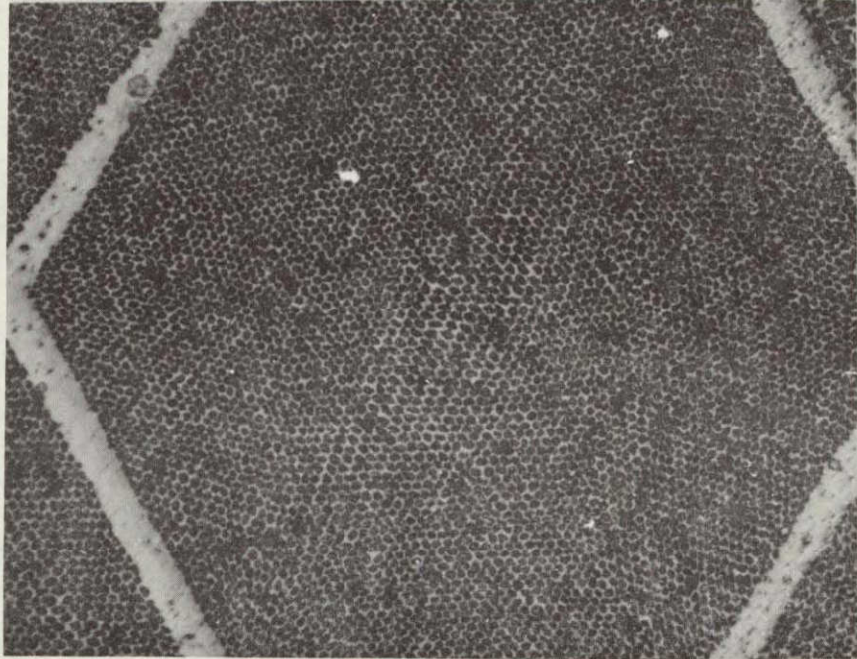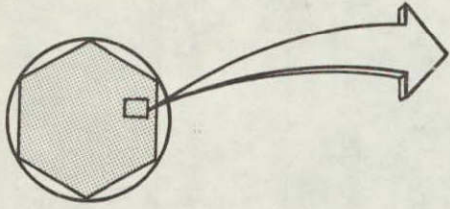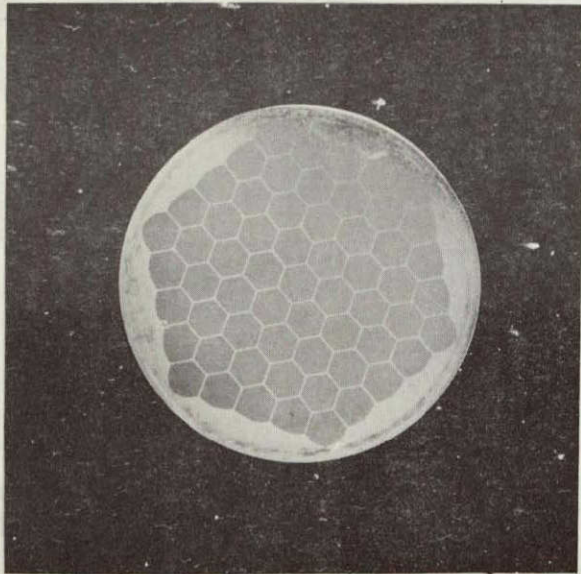
Figure 2-13 Collimated Hole Structure (CHS) Grid Magnified 65 Times

The first consideration in designing such a nozzle was to construct a contour that allows the flow to rapidly expand near the throat and then smoothly turns the flow back parallel to the centerline. The second consideration was the effect of the nozzle wall boundary layer on the expansions process. While the flow is in the continuum regime, classical boundary layer concepts can be used to estimate the growth of the displacement thickness and subsequently adjust the nozzle wall contour to maintain the desired expansion.

Nozzle flow separation is not a concern unless the back pressure in the telescope exceeds the pressure at the nozzle exit (i.e., the helium is overexpanded). As a general rule, the back pressure can exceed the nozzle exit pressure by a factor of two before the adverse pressure gradient in the boundary layer creates a reverse flow and separation or detachment from the wall can occur. Another situation that could lead to flow separation is if the displacement thickness begins to grow inward at a faster rate than the nozzle wall is expanding outward. This creates an effective convergent nozzle which would create adverse pressure gradients in the boundary layer and subsequent detachment of the flow from the nozzle wall. Because of the large displacement thickness that develops at low operating pressures, there is a certain expansion ratio where the displacement thickness increases faster than the wall expands and the nozzle is truncated at that point.

Wall contours were computed for 50:1, 100:1 and 200:1 expansion ratio nozzles using the bell nozzle design code described in Reference 6. Numerical values for a 100:1 nozzle contour are given in Appendix C. Because of the small scale required (throat diameter = 0.0312 inches (0.8 mm)), it was decided to use a short cylindrical throat region followed by a sharp corner expansion. A corner expansion at the throat produces a shorter nozzle design than a rounded or circular throat contour and obviously is easier to manufacture.

An evaluation of the boundary layer growth for a range of operating conditions was computed with the BLIMPK code (Ref. 7). The original code was modified to allow the helium to cool below 100 K during the expansion process. Room temperature helium

and helium cooled to liquid nitrogen temperature were considered as well as operating pressures from 0.01 to 0.001 atmospheres. Typical input data are illustrated in Appendix C.

Contour ① in Figure 2-14 illustrates a nozzle wall profile for a 100:1 expansion ratio nozzle. When viscous effects predicted by BLIMPK are superimposed, the effective wall contour is displaced inward as illustrated by contours ② , ③ and ④ in Figure 2-14. These results tend to indicate the potential problems with the use of low density nozzles for helium injection.

In an attempt to compensate for the rapid boundary layer growth, the nozzle wall contour was displaced outward an amount equal to the boundary layer displacement computed for 100 K helium at 0.01 atm total pressure (see contour ⑤). This produced a conical nozzle with a half angle of 25 degrees. If the nozzle is truncated at an expansion ratio of around 32 (M = 6.5), the nozzle should perform properly at a total pressure of around 0.01 atm (7.6 Torr).

2.4.3 Helium Flow Metering System – A schematic diagram of the flow measuring system is indicated in Figure 2-15. Flow rates through the helium purge supply line were measured with a 1/16" Fischer & Porter Tri-Flat variable area flowmeter with a sapphire ball. The pressure within the flow meter was maintained at around 22 psia and the temperature was monitored with a copper-constantan thermocouple.

To evaluate the experimental procedure and verify the calibration curves provided with the flowmeter, several test cases were run using the following procedure:

a)   pump down the chamber to 10^{-5} Torr,

b)   set up the helium flow meter to a prescribed flowrate while the diffusion pump is on-line , and then

c)   close the valve to the diffusion pump and monitor the chamber pressure rise-rate on an ionization gage calibrated for helium.

2-22
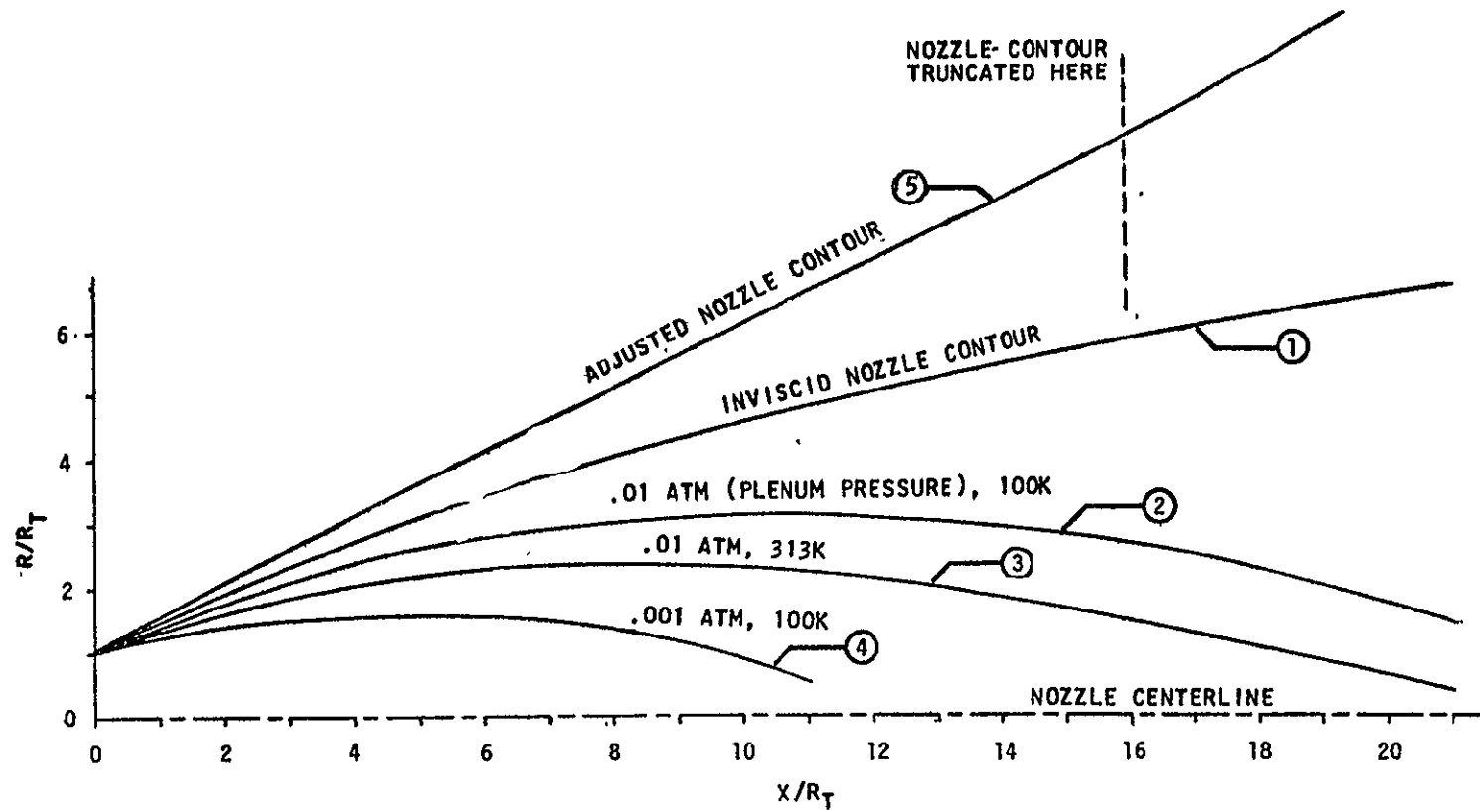
Figure 2-14 Calculated Nozzle Contours and Boundary Layer Displacement Thickness –
100:1 Expansion Ratio Nozzle
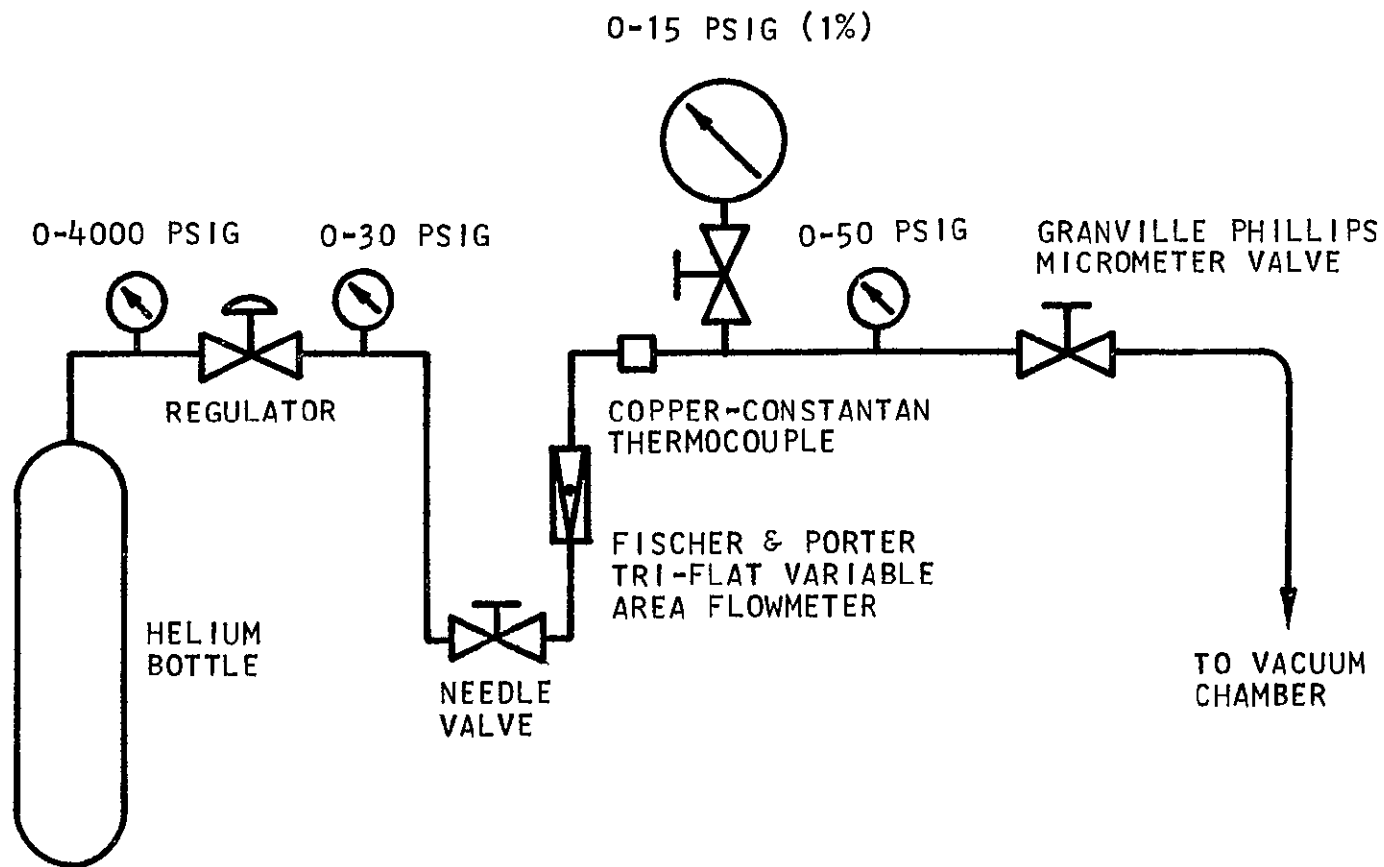
Figure 2-15   Helium Flow Metering System

The pressure rise rate in the chamber with the diffusion
pump off should be a function of the chamber volume and incoming
flowrate. The mass flowrate can be calculated using these parameters by the following relationship

$$\frac{dm}{dt} = \frac{VM}{RT}\frac{dp}{dt} \quad (g/s)$$

where V, the chamber volume, is $6.2 \times 10^6 \pm 0.1 \times 10^6$ cm^3 and

M = 4,
R = 62363 and
T = 300 $\pm$ 10K.

Although the thermocouple was operating, an ice bath was
not used for these runs so an actual temperature reading was
not obtained. The low flow rates and relatively long copper
lines which were at room temperature should have produced a helium
flow near room temperature. Figure 2-16 is a record of the chamber
pressure history when 3.3×10^{-4} g/s of helium was flowing into the
chamber. A separate run was made with all valves closed and no
helium flow to determine the chamber virtual leak rate which was
0.58×10^{-5} g/s. The table below compares the mass flow rates
indicated by the flowmeter and that inferred from the chamber
pressure rise rate. The comparison is within acceptable limits.

Flow Meter Data		Chamber Pressure Rise Rate Data (g/s) (corrected for leaks)	Percentage Contribution
Setting	Mass Flow (g/s)		
4	4.4×10^{-5}	4.4×10^{-5}	–
10	3.3×10^{-4}	3.4×10^{-4}	4

2.4.4 Purge Gas Plume Pressures – Plume mapping was conducted
to define the pressures within the telescope housing and between
the telescope aperture and ion beam source. Figure 2-17 illustrates the variation in telescope pressure and vacuum chamber
pressure as a function of helium flow rates. The telescope pressure was measured at a point 2.5 cm from the end plate using a

RUN 136 (12 MAY 78)

He FLOWMETER SET AT 10

P_{fm} = 22 psia

OPEN VALVE

CLOSE VALVE

$$\frac{dp}{dt} = \frac{5.6 \times 10^{-4} \text{ Torr } (5.32)}{11.2}$$

$$= 2.66 \times 10^{-4} \text{ Torr/Sec}$$

1.0 SEC

1×10^{-5} TORR
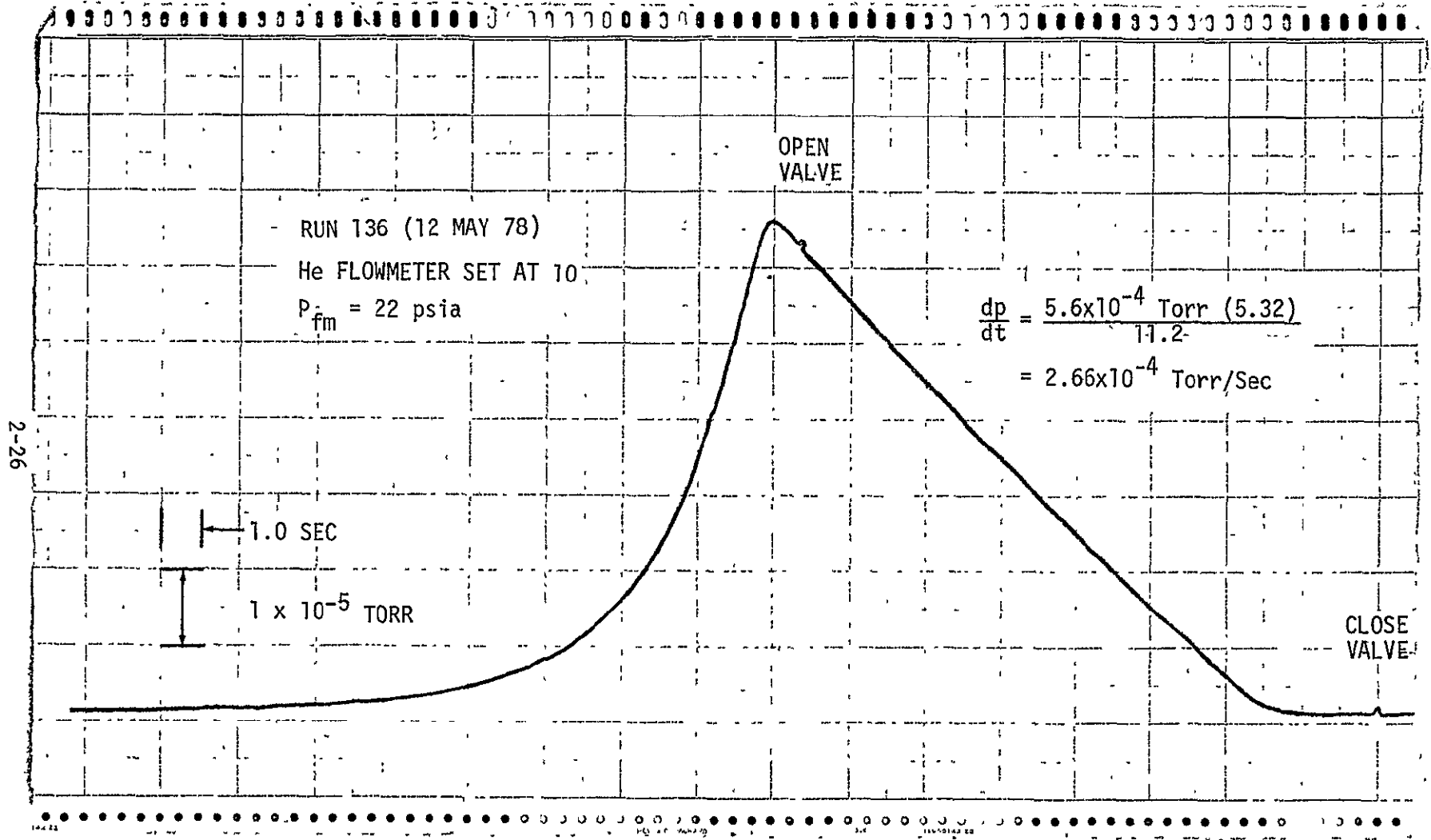
Figure 2-16   Chamber Pressure Rise-rate with Helium Flow
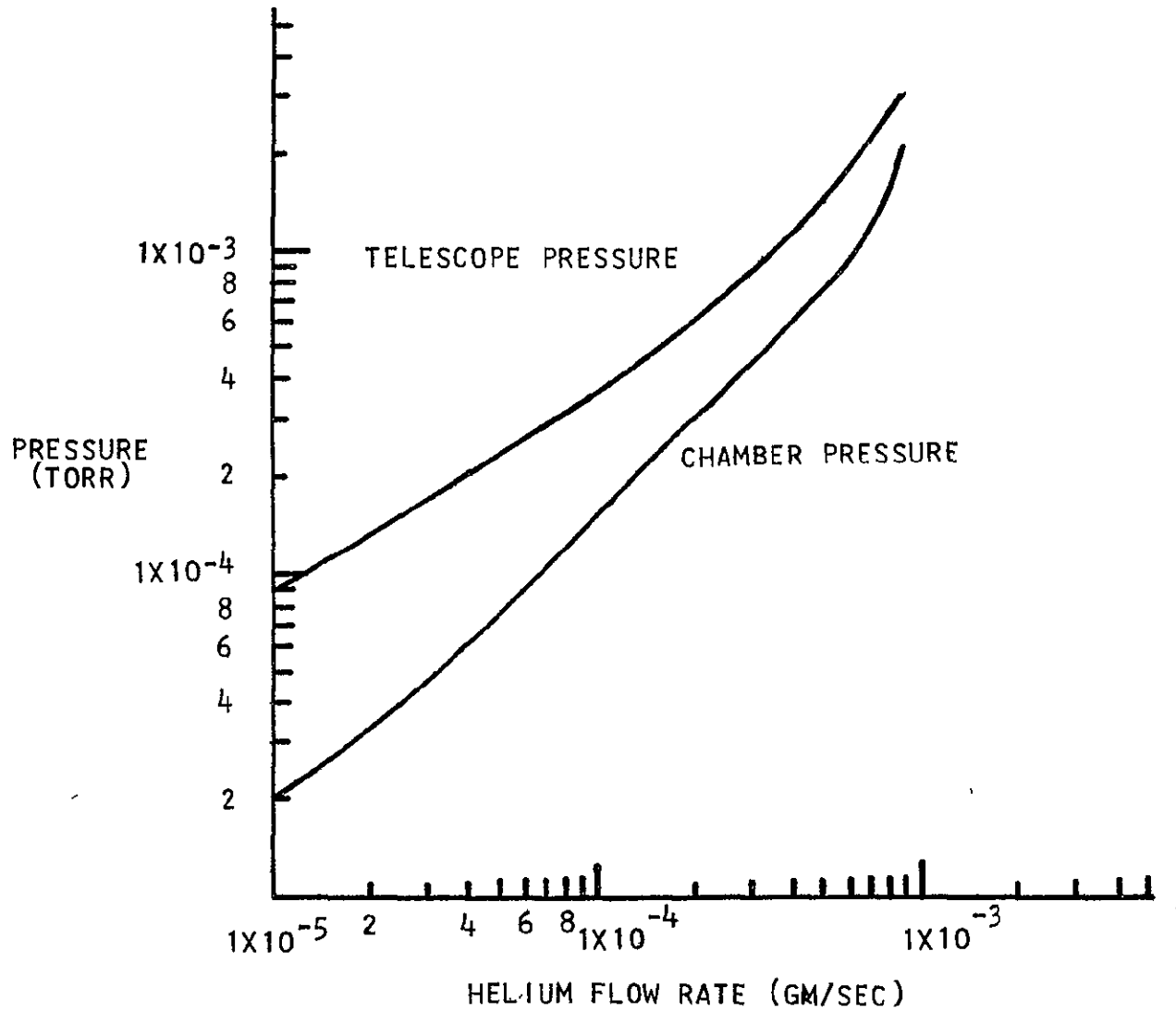
Figure 2-17 Telescope and Chamber Pressure Variation with Helium Flow Rate

Veeco ionization gage   The procedure for converting the gage
output to a helium pressure is discussed in Appendix E.

The helium flow out of the simulated telescope was measured
with a free molecular density probe that was moved across the
entrance of the telescope just outside the sunshade. The density
probe was a cylindrical volume which had a 1.27 cm diameter hole
drilled in the side that faced the helium flow as shown in
Figure 2-18. An ionization gage and thermocouple were mounted
to the side of the cylinder to monitor the pressure and tempera-
ture of the gas within the cavity.

The results of the helium plume mapping are shown in Figures
2-19 thru 21 for the diffuse source (i.e., the (CHS)) and the 25
degree half angle nozzle. As illustrated, the variation in the
plume density does not deviate significantly across the aperture
of the telescope. The axial variation along the telescope axis
between the ion source and the simulated plane of the primary
optics is also shown in the figures.

2.5 Ion Beam Detectors - Two different methods of detecting
the incoming beam of contaminant ions were employed. These are
discussed below.

2.5.1 Ion Current Measurements - Each of the three basic
components of the model telescope (i.e., the sunshade, barrel and
end plate) were isolated electrically. By grounding two of the
components to prevent charge buildup, the beam current collected
by the third component was measured with a Keithley 610A electro-
meter. Sensitivies for this instrument range from 1A to 10^{-12}A
full scale.

2.5.2 Mass Spectrometer - A Granville-Phillips Spectra
Scan 750 residual gas analyzer (RGA) was also used as a detec-
tion device. A quadrupole probe was mounted in the base of the
telescope model (Figure 2-12) in the plane of the primary optics.
The instrument can monitor partial pressures of neutrals or ions
in a range of operation from 10^{-4} Torr (N_2 equivalent) to 5×10^{-15}
Torr with mass numbers ranging from 1 to 750 amu. With the RGA
mounted in the same plane as the end plate of the model telescope
this allowed correlation between the RGA reading and the current
measured by the Keithley electrometer.

2-28

THERMOCOUPLE

IONIZATION GAUGE

INCOMING FLOW

INTERNAL SURFACE AREA OF CAVITY, 195 CM^2

A, AREA OF APERTURE, 2 CM^2
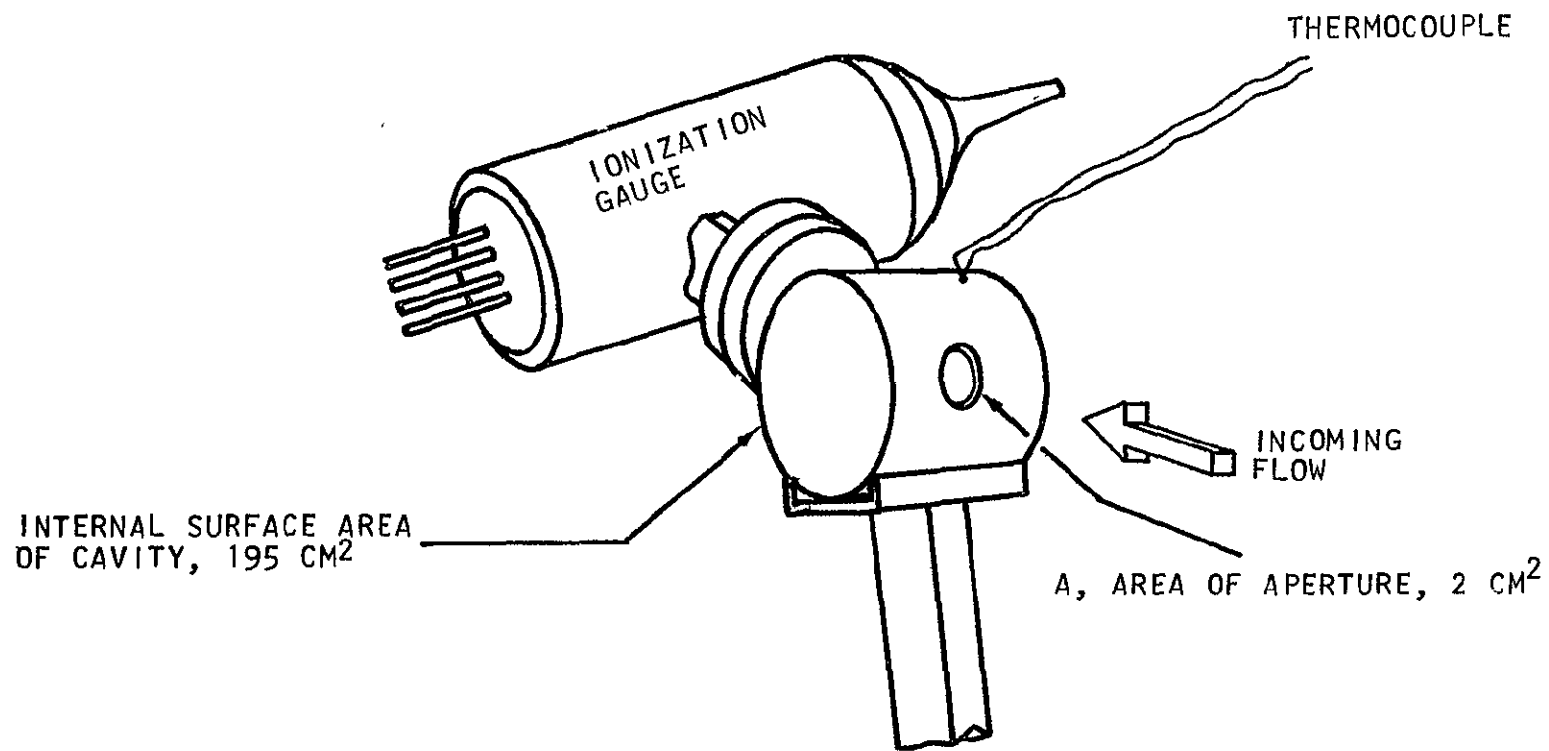
Figure 2-18 Sketch of Density Probe Used for Plume Mapping
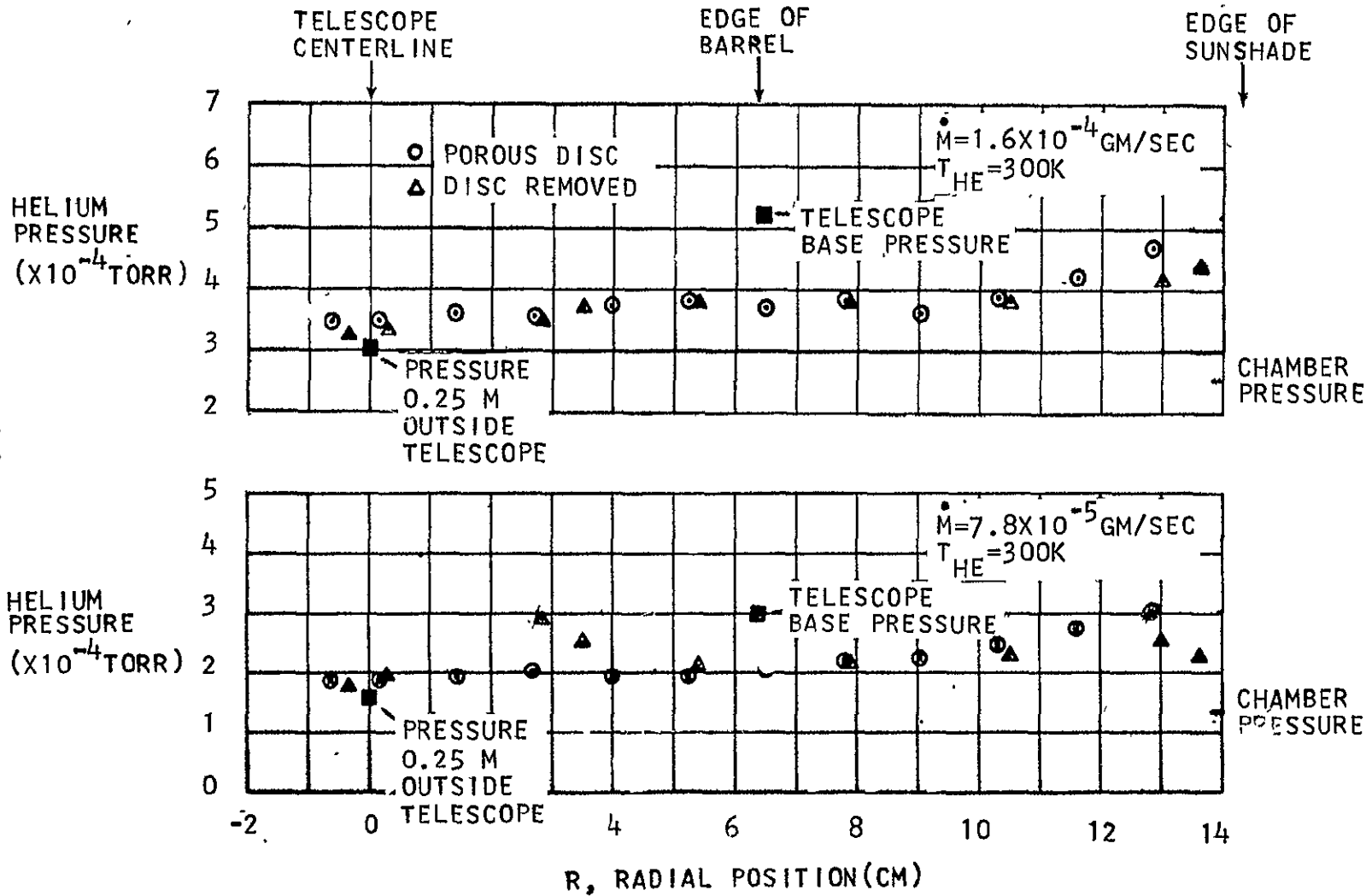
Figure 2-19   Helium Pressure Profile Across Telescope Aperture - Collimated Hole Structure Injection
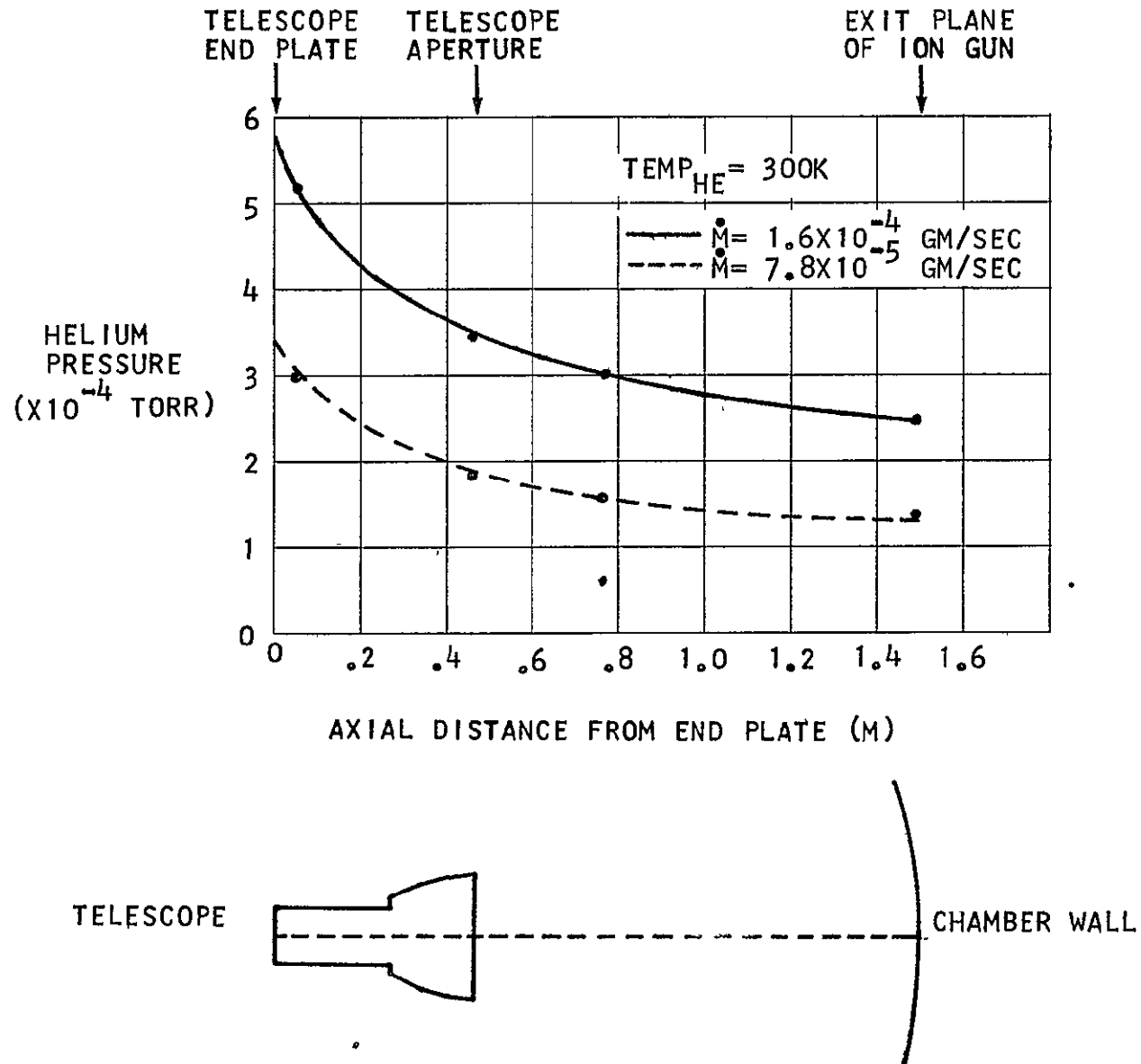
Figure 2-20 Axial Variation in Pressure
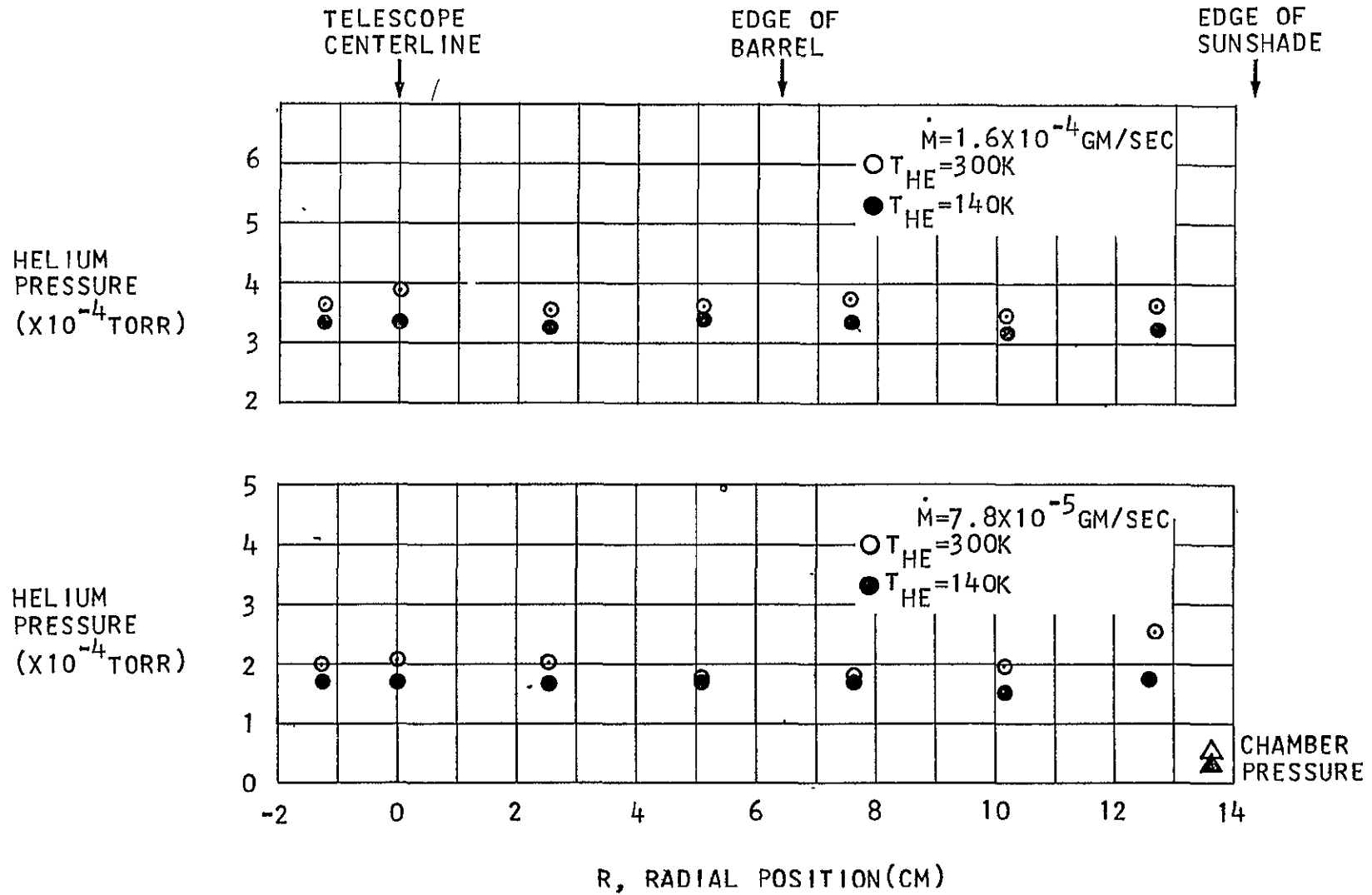
Figure 2-21 Helium Pressure Profile Across Telescope Aperture - Nozzle Injection

Prior to inserting the RGA probe in the chamber, a series
of baseline scans were made with the probe mounted externally on
a side flange of the chamber. This is the standard mode of opera-
tion and the existing coaxial cables could be used.
To operate the probe inside the chamber, new RF and high voltage
leads were required which altered the response of the system and re-
quired some internal adjustment to the electronics. Before making
the new electrical connections, a total of 25 scans were taken
of the residual gas in the chamber (with and without helium
flow in the chamber) at various settings of the following RGA
parameters:

- a) resolution,
- b) scan speed,
- c) strip chart paper speed,
- d) ionizing voltage,
- e) ionizing current,
- f) ion energy,
- g) lens voltage and
- h) electron collector voltage.

Since the mass spectrometer was designed to detect partial
pressures as low as 10^{-15} Torr, most of the controls had to be set
to desensitize the instrument. The RGA has an "Operate/Standby"
switch which in the standby mode removes the ionizing current.
With ions from the ion gun arriving at the quadrupole entrance,
there was no need to use the ionizing current. Switching back
and forth between the "operate/standby" mode provided an indi-
cation of the ratio of neutrals-to-ions that would reach the
base of the scale telescope.

3.0 TEST PARAMETERS

3.0 TEST PARAMETERS

3.1 Scaling Considerations – Based on discussions with Ames
Research Center personnel and the work of Murakami[1], a nominal
pressure of 5×10^{-6} Torr should theoretically provide the desired
contamination protection for a full scale telescope. To achieve
similar contaminant/helium interactions in the scale model tests,
the Knudsen number should be simulated. The Knudsen number is
defined as

$$KN = \lambda_{a-He}/L \qquad \qquad (3-1)$$

where

λ_{a-He} = mean free path traveled by the incoming species be-
tween collisions with the purge gas and

L = characteristic dimension of the telescope (distance
from aperture plane to primary optics).

When the velocity of the incoming contaminants is high relative
to the velocity of the purge gas, the mean free path can be ex-
pressed as

$$\lambda_{a-He} = \frac{1}{\sigma_{a-He} \, N_{He}} \quad (cm) \qquad \qquad (3-2)$$

where σ_{a-He} = collision cross section for a particular helium/
contaminant species interaction (cm^2) and

N_{He} = number density of helium (molecules/cm^3).

The number density of the helium can be expressed in terms of its
temperature and pressure

$$N_{He}' = \frac{9.7 \times 10^{18} \cdot P \; (Torr)}{T \; (K)} \; . \qquad \qquad (3-3)$$

Using a helium pressure of 5×10^{-6} Torr and a gas temperature of
20 K for the full scale telescope, a corresponding pressure can be
computed, for the one-tenth scale model which uses 300 K helium.

From equations (3-1), (3-2) and L_{fs} = 10 Lm, it follows that N_m/N_{fs} = 10, where subscripts m and fs denote model and full scale.

$$\text{Then,} \quad \left[\frac{P \ (\text{Torr})}{T \ (\text{K})} \right]_m = 10 \left[\frac{5 \times 10^{-6}}{20} \right]_{fs} \qquad (3\text{-}4)$$

If T_m = 300 K.

$$P_m = 7.5 \times 10^{-4} \text{ Torr.}$$

This indicates that the helium pressure inside the scale model telescope should be in the upper 10^{-4} Torr range to generate the same stopping capability of 5.0×10^{-6} Torr in the full scale SIRTF. Therefore using the Knudsen number scaling criteria, the pressure scaling relationship would be

$$P_{model} = 150 \cdot P_{full \ scale.} \qquad (3\text{-}5)$$

Another consideration in translating the subscale results to a full scale telescope is the distance over which collisions between contaminants and the helium purge gas take place. In the laboratory, this distance is only the distance between the ion source and the critical surface (1.5m), whereas in the full scale configuration, the collisions take place over the entire distance from the telescope to a point in space where the helium density is negligible.

One method of making this translation is to introduce an integrated or column density concept to represent the total number of collision sites encountered by the incoming contaminants. Assuming a single collision model it can be shown (see Reference 8) that the attenuation in the incoming flux is expressed as

$$I/I_o = e^{-\sigma \bar{N} \ell} \qquad (3\text{-}6)$$

where I_o is the ion beam current measured in the absence of the scattering gas. If the number density varies as a function of distance along the path length, ℓ,

$$I/I_o = e^{-\sigma \int_o^\ell N ds} = e^{-\sigma \cdot NCD} \qquad (3\text{-}7)$$

The integral is often referred to as the number column density (NCD) along the direction of the incoming flux. Both the subscale and full scale column densities integrated out along the telescope axis can be expressed in terms of pressure in the telescope measured at the base of the telescope.

Utilizing Figure 2-20 to approximate the axial variation in helium density between the ion source and the base of the telescope, an average number density for the one-tengh scale model can be determined from the perfect gas law, $P = N \cdot R \cdot T / N_a$,

where $R = 62363$
$N = $ molecules/cm^3
$N_a = 6.023 \times 10^{23}$
$T = $ temperature K

or $\overline{N} = 0.62 \cdot 6.0 \times 10^{18} \cdot P_{telescope} / T$. $\qquad$ (3-8)

where 0.62 is the averaging factor computed from the pressure distribution in Figure 2-20. The scattering length for the subscale configuration was 150 cm, therefore the number column density is

$$NCD = 9 \times 10^{20} \cdot P/T \qquad (3-9)$$

For the full scale configuration, some assumptions must be made concerning the plume expansion process. If the flow is free molecular at the telescope aperture, the density distribution in space will be approximately a cosine distribution (i.e. $N \propto \cos\theta/r^2$) (see Dushman[8]). If the flow is in the continuum regime at the telescope aperture, the expansion process would be self-confined and the density distribution would be more concentrated around the primary axis (i.e., $N \propto \cos^n\theta/r^2$, where $n > 2$. Murakami[1] assumed $n = 2$).

Because the mean free path of the helium purge gas will be on the order of the telescope dimensions, the continuum expansion model cannot be justified.

The number column density along the primary axis of the telescope can then be expressed analytically as described below. The helium mass flux arriving at a point P outside the telescope can be expressed as

$$\dot{m} = \int_0^{r_o} \int_0^{2\pi} \frac{\dot{m}_o \, r d\emptyset \, dr \, \cos^n\theta}{R^2} = \int_0^{r_o} \frac{2\pi \dot{m}_o \, r dr \, \cos^n \theta}{R^2} \qquad (3-10)$$
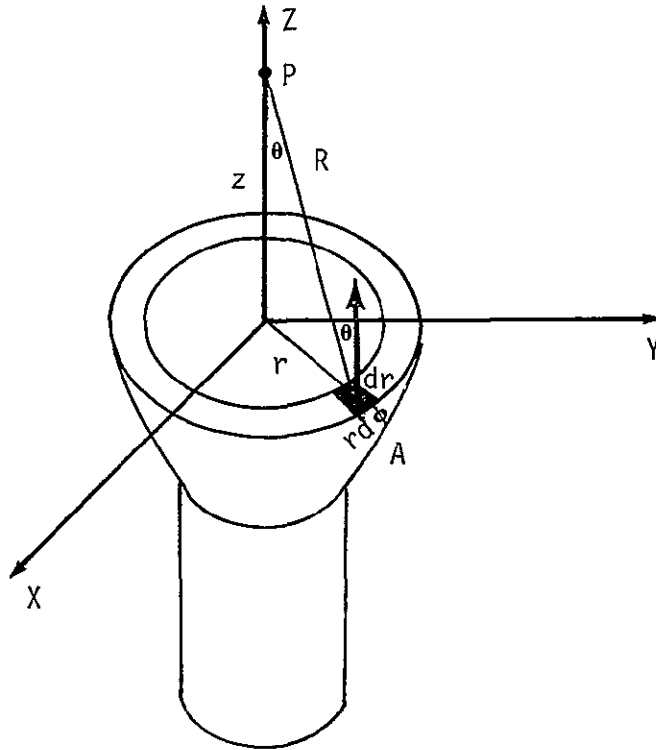
Figure 3-1   Sketch of Helium Flow from Telescope

where the flux from each elemental area emerges with a $\cos^n \theta$ distribution as depicted in Figure 3-1   and $\dot{m}_o$ is the total mass flow from the telescope divided by the aperture area.

Using $R^2 = Z^2 + r^2$ and $\cos \theta = Z/R$, equation 3-10 becomes

$$\dot{m} = \int_0^{r_o} \frac{2\pi \dot{m}_o \, rdr \, Z^n}{(Z^2+r^2)^{(n+\frac{1}{2})}} = \frac{2\pi \dot{m}_o Z^n}{(1-2n)} \left[\frac{1}{(Z^2+r_o^2)^{(n-\frac{1}{2})}} - \frac{1}{Z^{2(n-\frac{1}{2})}} \right] \quad (3-11)$$

For this free molecular flow model, the gas velocity has reached its limiting value, V_{max}, within the telescope. The mass density at point P is then

$$\rho = \dot{m}/v_{max}$$

and the mass flux at the aperture can be expressed as

$$\dot{m}_o = \rho_o v_{max} = \frac{P\ MW}{RT}\ v_{max}.$$

Converting the mass density to a number density and integrating along the Z axis, the number column density defined in equation (3-7) for the helium plume outside the telescope becomes, (3-12)

$$NCD_{outside} = \frac{N_a \cdot 2\pi\ P}{RT\ (2n-1)} \int_o^z \left[-\frac{z^n}{(z^2+r_o^2)^{(n-\frac{1}{2})}} + \frac{1}{z^{(n-1)}} \right] dz$$

for n = 1,

$$NCD_{outside} = \frac{2\pi\ N_a P}{RT} \int \left[1 - \frac{z}{(z^2+r_o^2)^{\frac{1}{2}}} \right] dz \qquad (3-13)$$

which, evaluated at values of Z which are large relative to the radius of the telescope r_o, becomes

$$= \frac{2\pi\ N_a P}{RT} \left[Z - \left\{ \sqrt{z^2+r_o^2} - r_o \right\} \right] \qquad (3-14)$$

$$NCD_{outside} = 2\pi\ r_o\ \frac{N_a P}{RT} = 3.0\text{x}10^{21}\ P/T \qquad (3-15)$$

In addition to the scattering sites created by the helium plume outside the telescope, the primary optics will also benefit from the helium that resides within the telescope barrel. Scattering that occurs within the telescope, however, will not prevent deposition on the cryogenic folding mirrors and baffles.

This internal contribution to the NCD can be defined in terms of the telescope pressure as

$$NCD_{inside} = \overline{N} \cdot \ell = \rho \frac{N_a \ell}{MW} = \frac{P}{RT}\ N_a \cdot \ell$$

$$NCD_{inside} = \frac{P}{RT}\ N_a \cdot \ell = 4.7\text{x}10^{21}\ P/T \qquad (3-16)$$

The sum of the two contributions to the full scale NCD is then

$$NCD_{total} = 7.7 \times 10^{21} \; P/T. \tag{3-17}$$

Equating equations (3-9) and (3-17) indicates that when a 300K helium purge is used in the scale model and a 20K gas in the full scale telescope, the pressure scaling relationship based on the number column density is

$$P_{model} = 128 \cdot P_{full \; scale} \tag{3-18}$$

3.2 <u>Energies and Fluxes</u> – The energy of the incoming contaminant molecules is an important parameter in determining the stopping efficiency of the helium purge gas. The ambient species at low orbital spacecraft altitudes (near 400 km) will have their own thermal velocities in addition to the relative orbital velocity with respect to the spacecraft (7.65 km/s). Table 3-I shows the calculated velocities and corresponding energy for different ambient gases at two temperatures relating to the medium and high density atmospheric models at a 400 km altitude. The thermal component has been added to the orbital velocity to represent the highest energy possible for the ambient atmosphere molecules. The energies corresponding to the 1800K thermal situation represent the worst case of the values as presented in Table 3-I.

The energy of the H_2O molecules that originate from the Shuttle Orbiter and are scattered back to the telescope will be a function of the number of collisions with the ambient atmosphere and the energy transferred during the collisions. The H_2O molecules leaving the Shuttle Orbiter have velocities relative to the Orbiter between 400 and 1000 m/s depending upon if they are emitted at thermal velocities (400 m/s) or from the flash evaporator (1000 m/s). The velocity of the ambient molecules relative to the Orbiter are shown in Table 3-I.

As a worst case for the testing, the water molecule was assumed to be scattered into the telescope at orbital velocities so that the helium purge could be evaluated for the maximum energy case.

3-6

Table 3-I Contaminant Gas Energies and Velocities

Orbital Velocity	Energy (Orbital)
N_2 7.65×10^5 cm/s	8.36eV
N 7.65×10^5 cm/s	4.18eV
O_2 7.65×10^5 cm/s	9.55eV
O 7.65×10^5 cm/s	4.78eV
H_2O 7.65×10^5 cm/s	5.38eV
Medium Density Thermal Velocity (1300K) Plus Orbital	Energy (Orbital + Thermal) *
N_2 $8.79 \times 10^4 + 7.65 \times 10^5 = 8.53 \times 10^5$ cm/s	10.4eV
N $1.24 \times 10^5 + 7.65 \times 10^5 = 8.89 \times 10^5$ cm/s	5.7eV
O_2 $8.22 \times 10^4 + 7.65 \times 10^5 = 8.47 \times 10^5$ cm/s	11.8eV
O $1.16 \times 10^5 + 7.65 \times 10^5 = 8.81 \times 10^5$ cm/s	6.4eV
High Density Thermal Velocity (1800K) Plus Orbital	Energy (Orbital + Thermal) *
N_2 $1.03 \times 10^5 + 7.65 \times 10^5 = 8.68 \times 10^5$ cm/s	10.8eV
N $1.46 \times 10^5 + 7.65 \times 10^5 = 9.11 \times 10^5$ cm/s	6.0eV
O_2 $9.68 \times 10^4 + 7.65 \times 10^5 = 8.62 \times 10^5$ cm/s	12.2eV
O $1.37 \times 10^5 + 7.65 \times 10^5 = 9.02 \times 10^5$ cm/s	6.7eV

* Thermal velocities have been added to orbital velocities to obtain
  maximum energy

3-7

Table 3-II Ambient Atmosphere Flux at 400 km

Orientation of Opening	Low Density Atmosphere (700 K)	Medium Density Atmosphere (1300 K)	High Density Atmosphere (1800 K)
Perpendicular	9.8×10^{12} particles/cm^2/s	1.6×10^{14} particles/cm^2/s	5.4×10^{14} particles/cm^2/s
Parallel	2.8×10^{9} particles/cm^2/s	5.74×10^{12} particles/cm^2/s	2.2×10^{13} particles/cm^2/s

The flux of ambient atmosphere gases on the telescope open-
ing, perpendicular and parallel to the velocity vector are shown
above in Table 3-II. The flux parallel to the flow is based on
the thermal energies of the ambient atmosphere alone. The low
density atmosphere corresponds to nighttime near a sunspot mini-
mum and the high density is for daytime near a sunspot maximum
(Reference 9).

Testing during this study showed that for a 10eV N_2^+ beam
at 1.5 meters from the ion gun, currents on the order of
2×10^{-9} A/cm^2 can be obtained. This equates to 1×10^{10} particles/
cm^2/s which is several orders of magnitude below on-orbit condi-
tions.

The effect of the ion flux levels was investigated to determine
if the stopping efficiency of a given flow of purge gas was in-
fluenced by this variation. The flux of N_2^+ ions was changed an
order of magnitude by adjusting the ion gun parameters. No
measurable change in the I/I_0 ratio was observed indicating that
simulating the magnitude of the on-orbit flux was not a major con-
sideration.

The mass flux of helium out of the scale model telescope is
on the order of 1×10^{-4} g/s or 1.2×10^{17} atoms/cm^2/s. The ratio
of helium flux from the scale model telescope to the contaminant
ion flux is 1.2×10^{7}. On-orbit, the same ratio will range from
1.2×10^{4} to 2×10^{2} which is between the low and high density at-
mospheres.

3-8

3.3 <u>Test Procedures</u> – The following steps outline the procedures used in establishing an ion beam and helium purge flow during a test.

- When the main chamber pressure is less than 10^{-5} Torr – establish gas source flow into the ion gun chamber at 100 microns.

- Set the ion gun filament current near 18 A for the 20 mil filament.

- Turn the filament-to-anode voltage to 150 volts.

- After an arc is initiated, reduce anode current to approximately 0.5 A by reducing filament current and/or anode voltage,

- Set the accelerator voltage to desired level.

- Set magnet at predetermined fixed current (near 1.5 to 2 A).

- Set the velocity filter voltage to predetermined value for the gas specie and velocity desired.

- Maximize ion beam to detector by adjusting deflector plate voltage, focusing electrode voltage filament current and anode voltage settings.

- Once steady beam results, record all parameters, including pressures and admit helium flow at various stepwise levels.

- Record ion current values at each helium pressure as well as helium flow rate, chamber pressure and telescope pressure.

- Periodically shut off helium flow to determine baseline current shifts.

- Continue helium pressure increases until the chamber pressure reaches 1×10^{-3} Torr.

4.0 TEST RESULTS

4.0 TEST RESULTS

4.1 N_2^+ Results – Collimated Hole Structure Injection – Using
the collimated hole structure as the mode of injecting the purge
gas into the telescope, N_2^+ ions were directed into the telescope
with velocities ranging from 7.8 km/s (9 eV) to 20.5 km/s (60 eV).
Figure 4-1 illustrates the attenuation in the ion current observed
at the base of the telescope as a function of the pressure measured
near the simulated plane of the primary optics. As indicated,
the higher velocity ions were attenuated less than the slower ions.

Also shown in Figure 4-1 is a plot of the N_2^+ ion attenua-
tion when air was used as the stopping medium. It is interesting
to note that the stopping efficiency of air was much greater than
helium. This could be attributed to its increased molecular
weight but more probably is associated with a charge-transfer
interaction that would also cause the disappearance of the N_2^+
ion current.

The open symbols in Figure 4.1 denote the results of tests
conducted with the purge gas and telescope surfaces at room tempera-
ture (300K ± 10K). Solid symbols are used to indicate the re-
sults of tests conducted with the helium and telescope surfaces
at 140K ± 10K. No significant difference was observed between
the hot and cold gas cases for a given mass flow of helium thru
the collimated hole structure injector.

It should be mentioned at this point that the pressure in
the telescope was monitored with an ionization gauge and therefore
was not a true measure of the gas pressure at 140K. A more de-
tailed discussion of this point is provided in Appendix E. If
the actual pressures (or momentum flux to a surface) had been
measured, the cold gas pressures would have been 0.47 lower.

For convenience in comparing the N_2^+ results with other ions,
a line drawn through the 10.8 eV data will be referred to as the
baseline attenuation. Figure 4.2 is a plot of the 8.7 km/s
attenuation data as a function of the average number density of
the scattering gas between the detector and source assuming the
static temperature of the gas was 300K. Although the experi-
mental configuration was not designed for cross section

4-1

SYMBOL	RUN NO.	STOPPING MEDIUM	ION	VELOCITY (Km/s)	ENERGY (eV)	TEMPERATURE (K)
⊙	168	HELIUM	N_2^+	7.8	9.0	300
△	169	HELIUM	N_2^+	10.0	15.0	300
◇	172	HELIUM	N_2^+	18.7	50.0	300
⬡	154	AIR	N_2^+	20.5	59.5	300
●	182	HELIUM	N_2^+	8.7	10.8	140
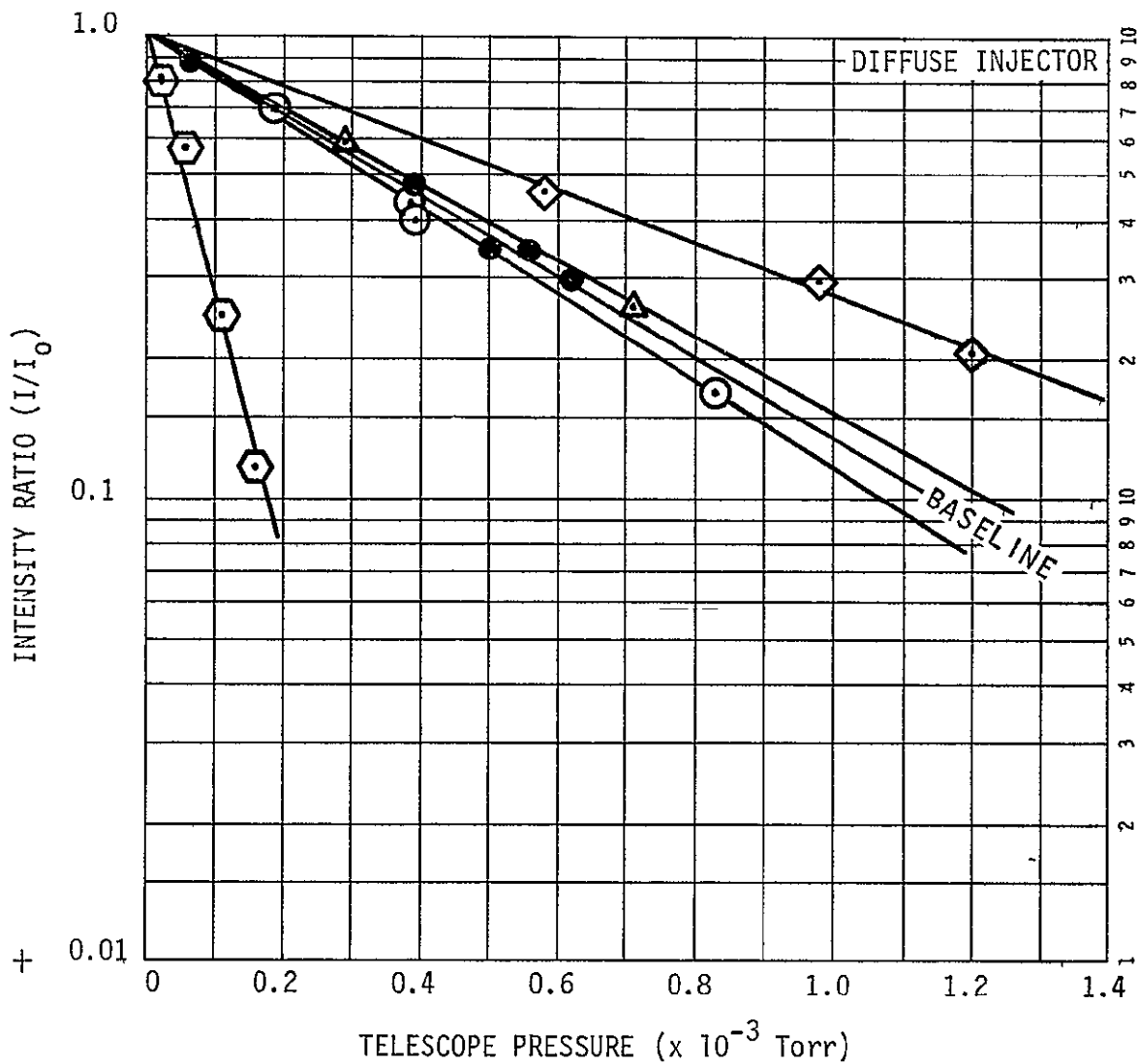
Figure 4-1 N_2^+ Beam Attenuation Versus Pressure
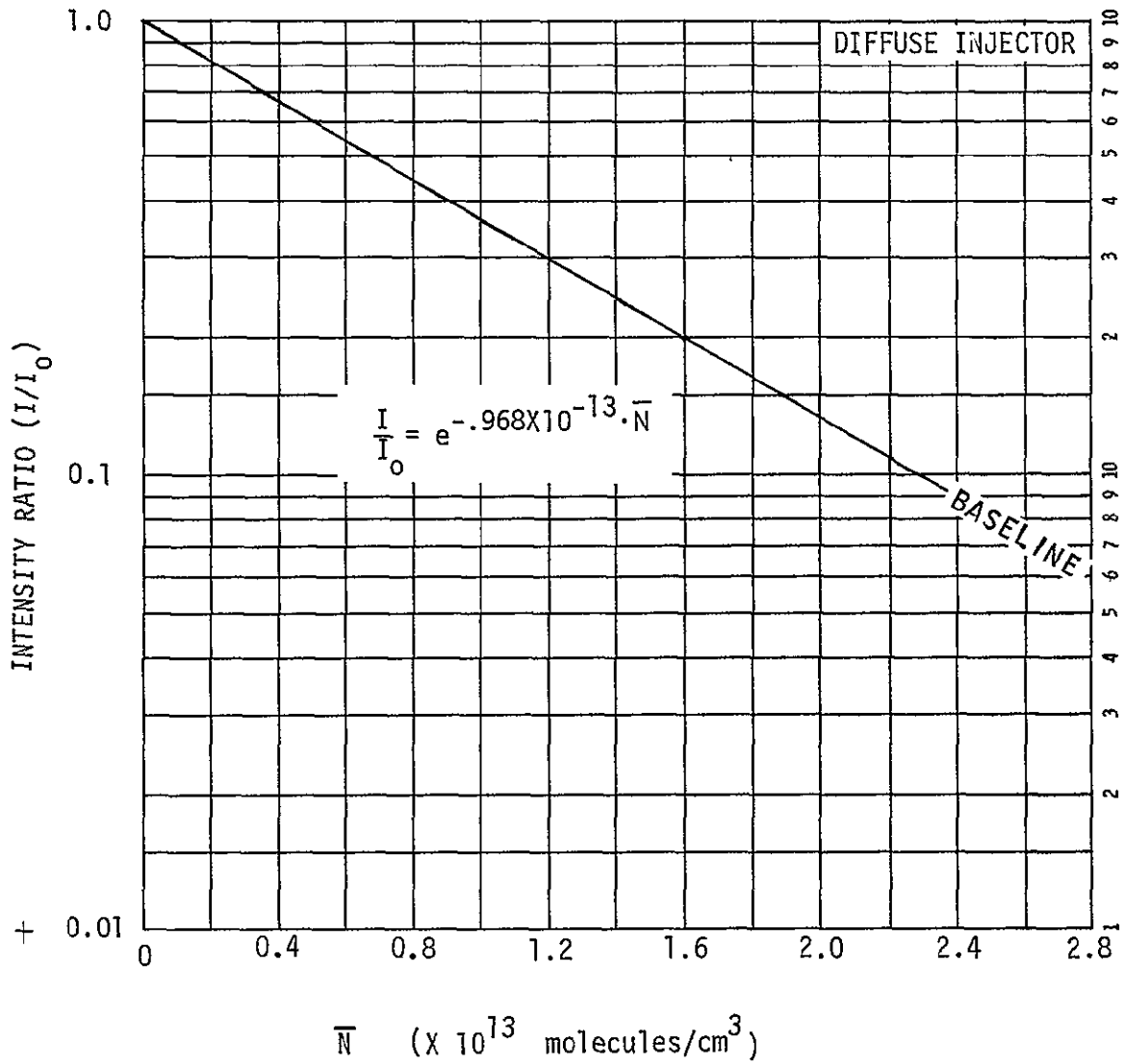
Figure 4-2 8.7 Km/s N_2^+ Ion Attenuation Versus Average Helium Number
Density Between Source and Detector

measurements, a comparison to previously published cross section
data was attempted. The experimental data in Figure 4-2 is cor-
related by the following relationship:

$$I/I_o = e^{-.968 \times 10^{-13} \cdot N}$$

(4-1)

Equation (4-1) can be used to infer that the incomplete collision
cross section for the N_2^+/helium interaction was 6.45×10^{-16} cm^2.
No attempt has been made to correct the incomplete cross section
for beam divergence, or beam size relative to the detector. How-
ever Bates[10] discusses the procedure for analyzing experimental
data and illustrates the importance of correcting for beam width
as shown in Figure 4-3. The open circles in the figure are the
experimental data of Simons et. al.[11] for H$^+$ scattering in
helium. The dashed curve is the cross section for the interaction
assuming an infinitesimally narrow beam and the solid curve is
the correction the beams finite width. The closed circle repre-
sents the baseline cross section data derived in equation (4-1)
from the N_2^+/helium data of this test. Considering this is a
comparison of different ions observed with different experimental
techniques, the excellent correlation is fortuitous - nevertheless
it does indicate the present N_2^+/Helium interaction at 10.8 eV
was reasonably similar to that previously observed.
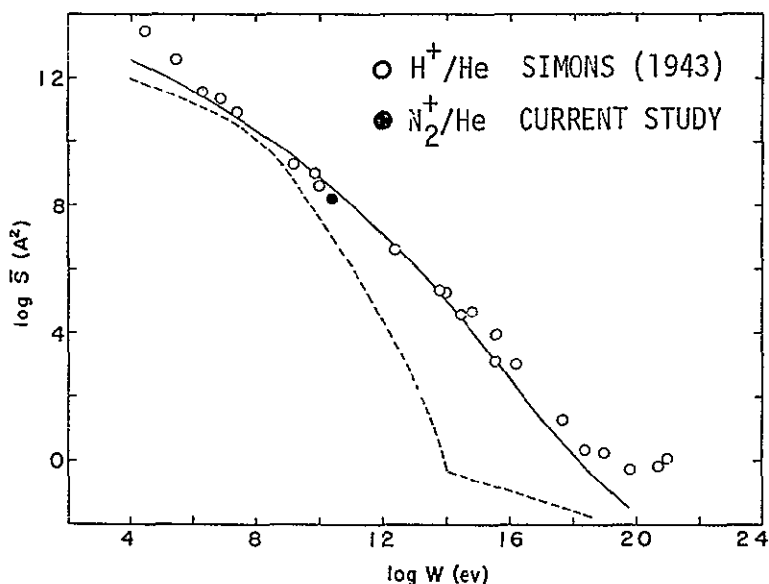
Figure 4-3 Comparison of Present Results with Earlier Observations of Simons[11]
(Taken from Reference 10)

A more useful presentation of the data is to plot the attenuation as a function of the helium number column density that existed between the source and base plate of the telescope as shown in Figure 4-4. The data indicate that to achieve an order of magnitude decrease in the N_2 flux, a helium column density of around 3.4×10^{15} molecules/cm^2 was required in the model configuration. A two order of magnitude decrease could be achieved by single collisions with a column density of around 6.6×10^{15} molecules/cm^2.

Using the scaling considerations derived in Section 3.1 (i.e. equation 3-17), the pressure required in the full scale telescope would have to be around 8.8×10^{-6} Torr to affect an order of magnitude decrease in the N_2 flux incident on the primary optics. This is slightly higher than that predicted by Murakami[1].

4.2 N_2^+ Results - Nozzle Injection - The low density nozzle described in Section 2.4.2 was also used as a method of injecting the helium purge gas. Figure 4-5 contains the results of tests where 8.7 km/s N_2^+ ions were attenuated by both the warm and cold helium purge flows. As illustrated there appears to be a slight increase in the effectiveness of the 300K gas compared to the 140K gas for a given helium mass flow rate. As discussed in Appendix E, the measured telescope pressure was not a true pressure at 140K. The limiting velocity of the 300K helium is 9.8×10^4 cm/s whereas the 140K would be 6.7×10^4 cm/s or a factor of 0.68 lower.

Although the same limiting velocities apply to the flow from the collimated hole structure, the nozzle was intended to direct more of the helium momentum in the axial direction so the effect may be more pronounced.

4.3 O^+ Results - O^+ ions were generated in the same fashion as the N_2^+ ions. Figure 4-6 shows the attenuation of the ion beam as a function of helium pressure. The attenuation is slightly less than that for N_2^+ and the reason is not fully understood. From a momentum consideration, the heavier N_2^+ ions should have been attenuated less than the O^+.

$$\frac{I}{I_0} = e^{-.693 \times 10^{-15} \cdot NCD}$$

INTENSITY RATIO (I/I_0)

NCD   (X 10^{15} molecules/cm^2)

DIFFUSE INJECTOR

BASELINE
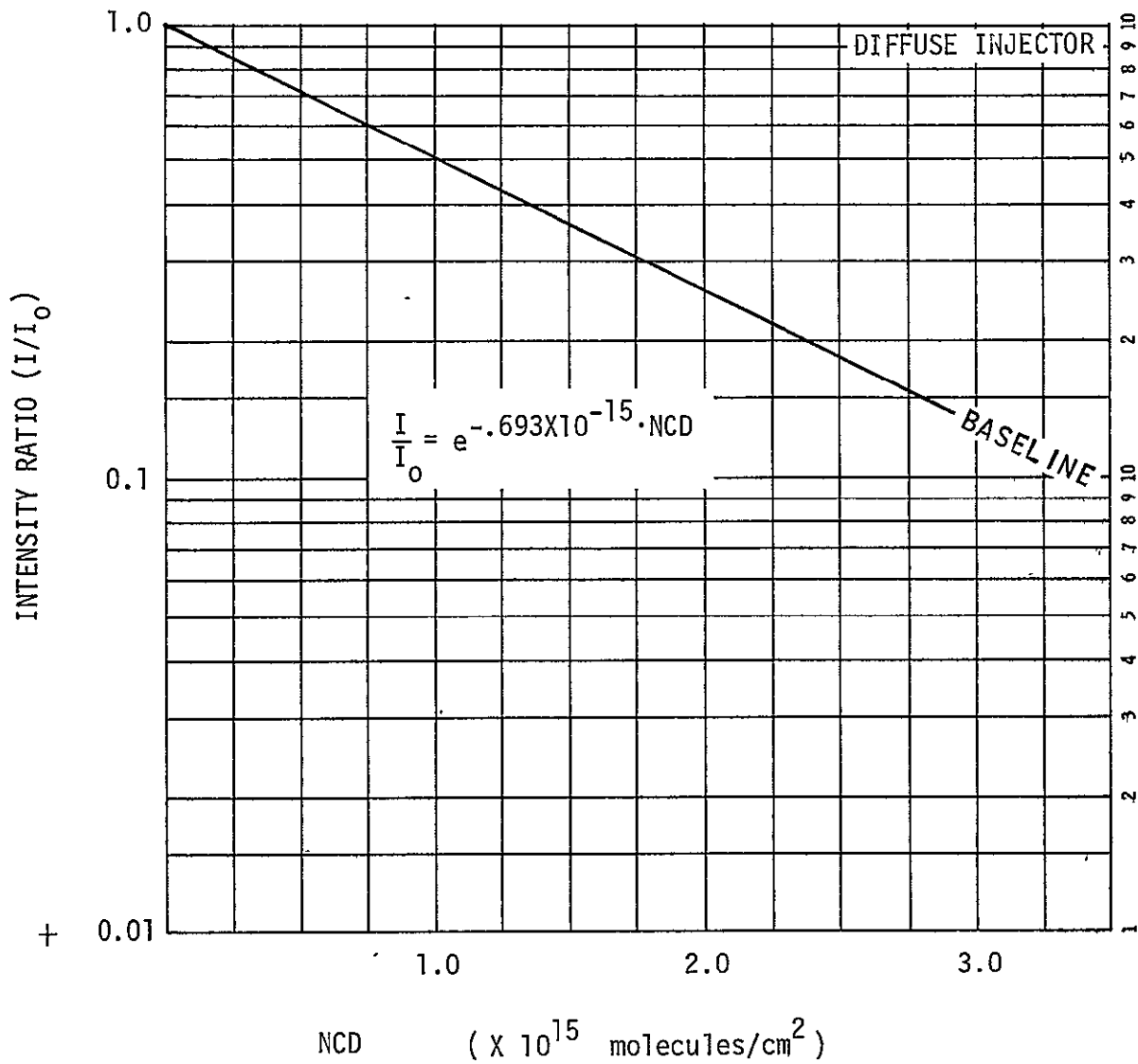
Figure 4-4   8.7 Km/s N_2^+ Ion Attenuation Versus Helium Number Column Density

SYMBOL	RUN NO.	STOPPING MEDIUM	ION	VELOCITY (Km/s)	ENERGY (eV)	TEMPERATURE (K)
●	184	HELIUM	N_2^+	8.7	10.8	140
○	183	HELIUM	N_2^+	8.7	10.8	300
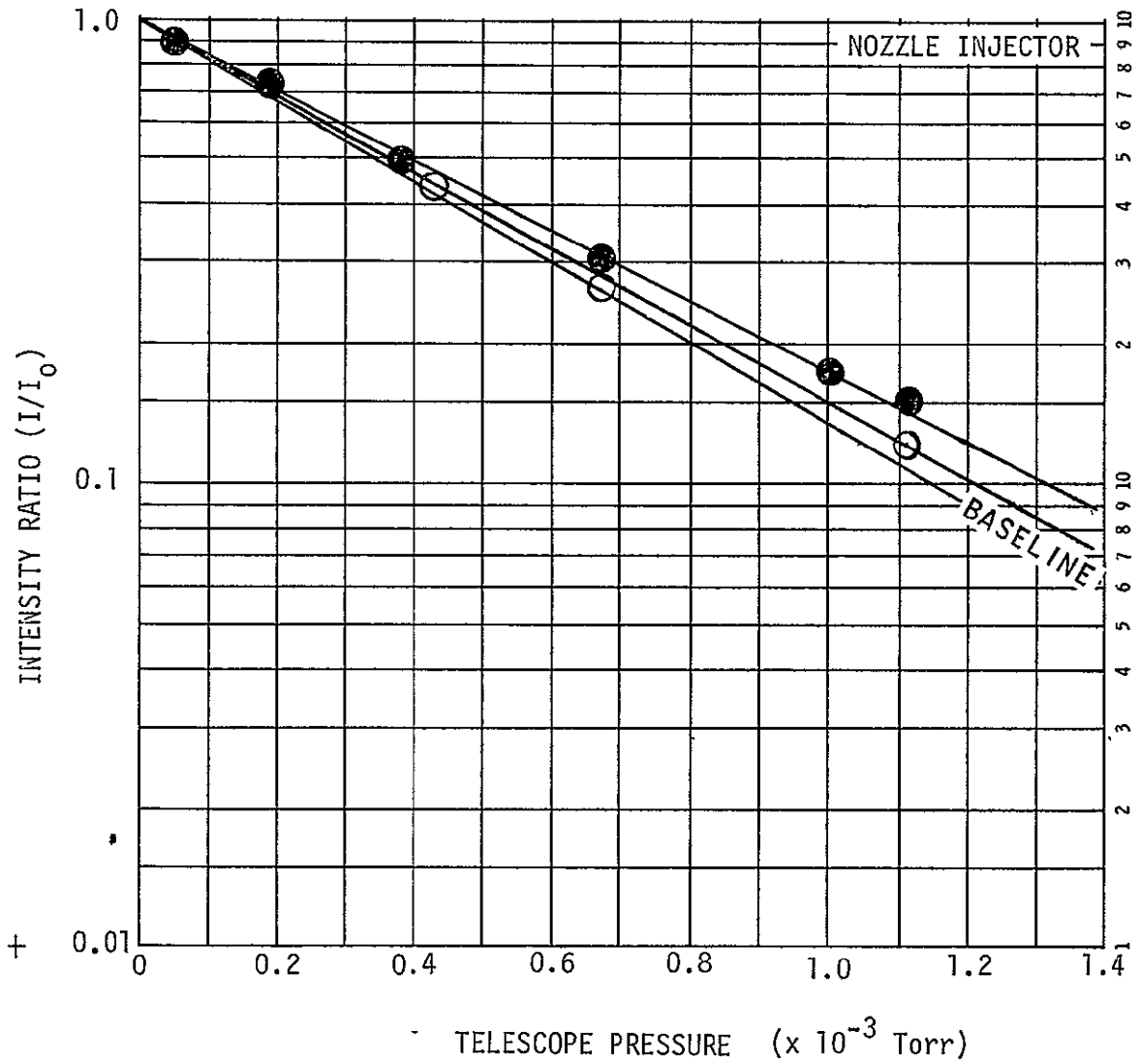
Figure 4-5 N_2^+ Attenuation Versus Pressure

SYMBOL	RUN NO.	STOPPING MEDIUM	ION	VELOCITY (Km/s)	ENERGY (eV)
⊙	164	HELIUM	0^+	7.4	4.5
△	163	HELIUM	0^+	8.7	7.0
◇	156	AIR	0^+	17.1	24.7
⬡	155	AIR	0^+	21.0	34.7
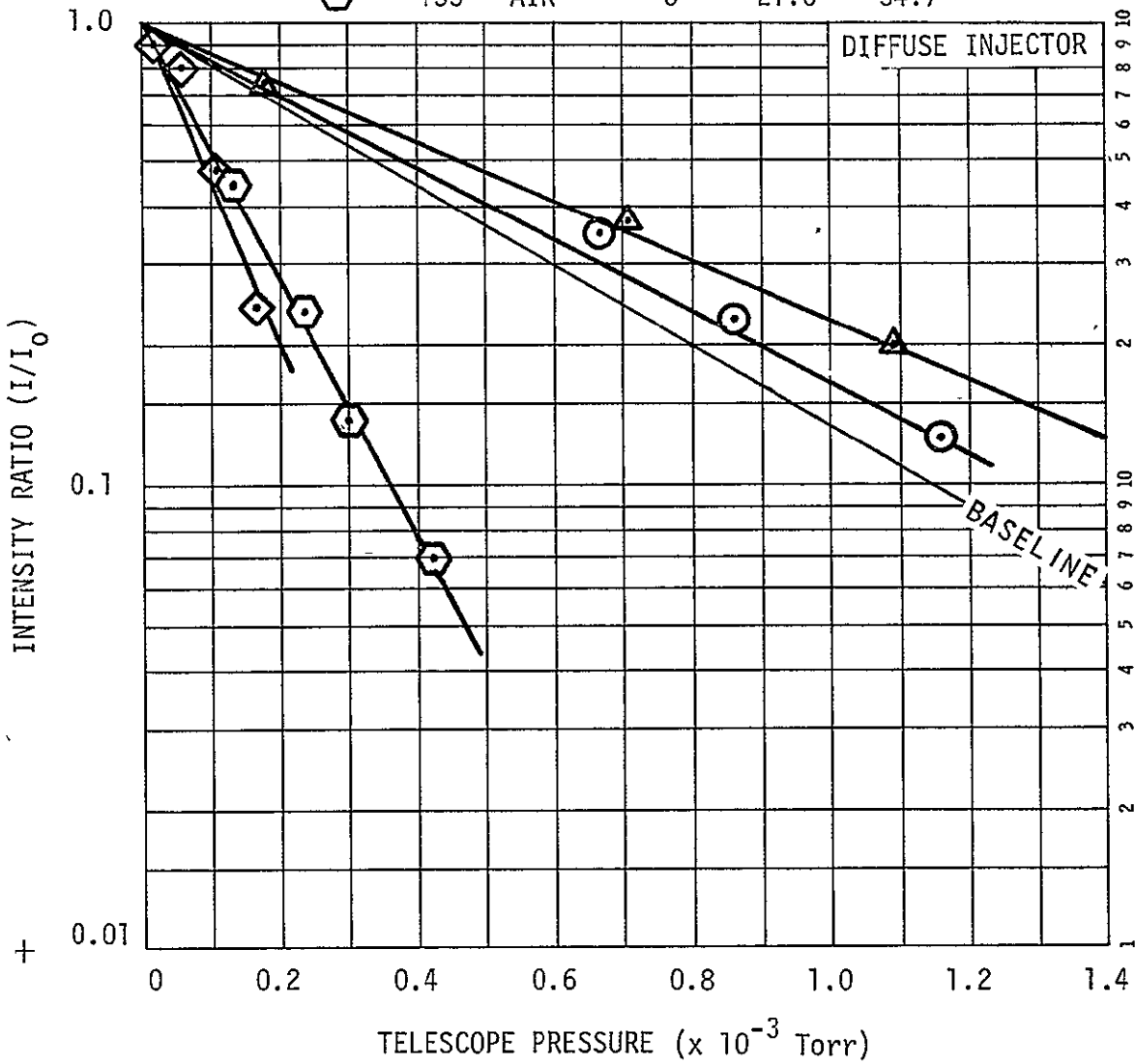
Figure 4-6 0^+ Beam Attenuation Versus Pressure

Also shown in Figure 4-6 are several runs where air was used as the stopping medium. For these two runs, the most energetic beam showed the least attenuation as expected.

4.4 H_2O^+ Results - H_2O^+ ions were used as an incident beam in the same manner as the N_2^+ and O^+ ions. Figure 4-7 shows the results at several velocities representative of expected on-orbit conditions. The H_2O^+ data is very similar to the O^+ data. It does show slightly less attenuation than the N_2^+ data.

4.5 O_2^+ Results - O_2^+ was investigated as an additional source. Figure 4-8 shows the attenuation for a 10.8 km/s beam with room temperature helium as the stopping medium. The O_2^+ curve is the same as the curve for 10.0 km/s H_2O^+ and shows less attenuation than the O^+ beam at 8.7 km/s.

4.6 Neutral Species Detection Results - An attempt was made to observe the high velocity neutrals that were reaching the end of the telescope. It can be hypothesized that some ions were neutralized by charge-exchange collisions with the residual gases in the chamber prior to entering the telescope or by direct collisions with the telescope walls or by a charge exchange interaction with a previously neutralized ion. The neutral species would not be observed as an electrically current so another technique utilizing a mass spectrometer was employed.

The mass spectrometer located in the base of the telescope was utilized in two modes of operation

a) simply as an ion filter and detector when the ionizing circuit of the RGA was inactive, and

b) as a normal mass spectrometer with ionizing filament operating.

In either mode of operation, the instrument could scan a range of mass numbers or be locked onto a specific ion. Figure 4-9 illustrate the output from the RGA using the automatic scan when the ionizing circuit was not operating but N^+ ions from the ion gun were directed into the telescope. Helium was then injected into the telescope at various rates. To verify the observed

SYMBOL	RUN NO.	STOPPING MEDIUM	ION	VELOCITY (Km/s)	ENERGY (eV)
⊙	166	HELIUM	H_2O^+	7.6	5.4
△	167	HELIUM	H_2O^+	10.0	9.4
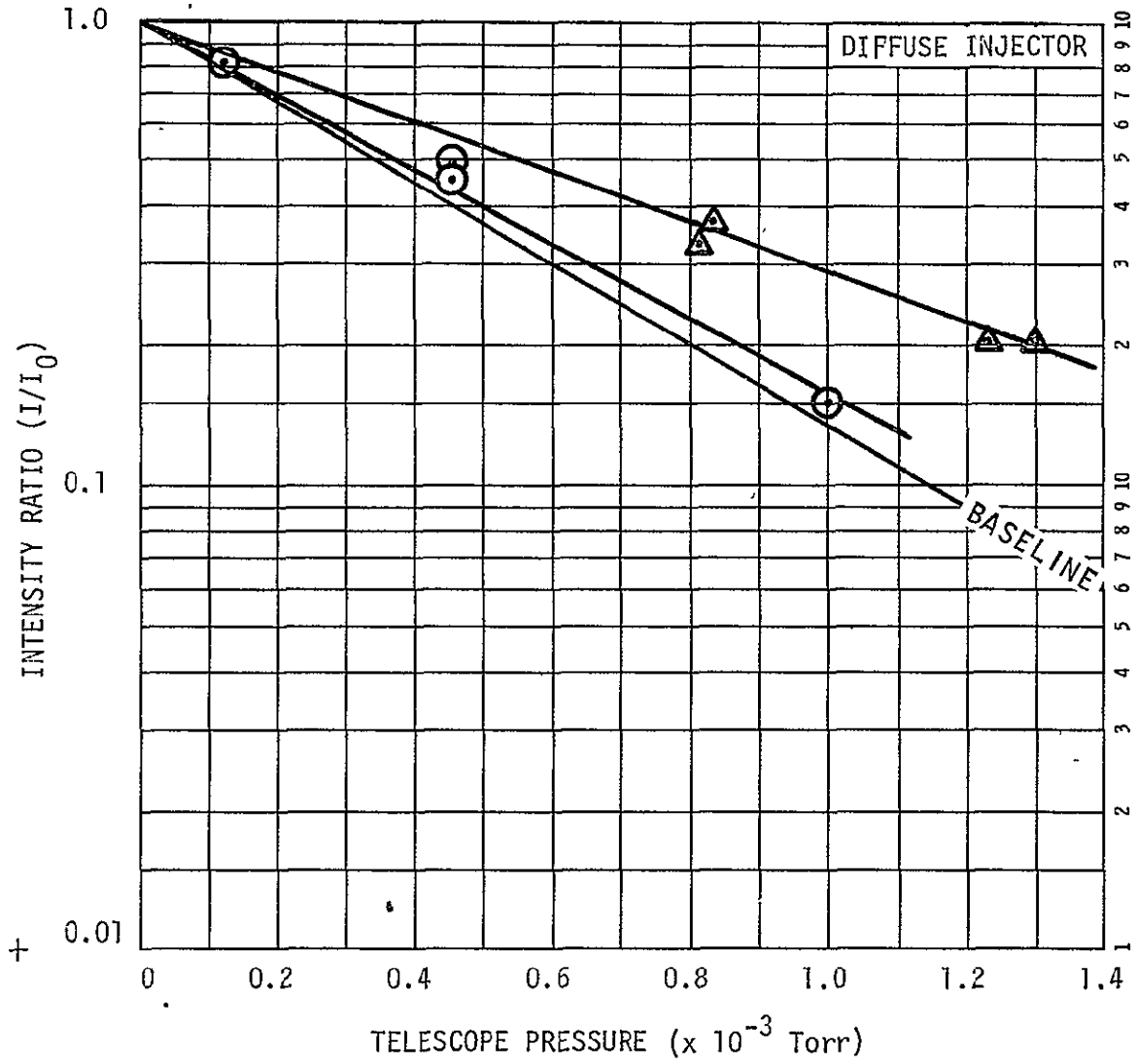
Figure 4-7 H_2O^+ Beam Attenuation Versus Pressure

SYMBOL	RUN NO.	STOPPING MEDIUM	ION	VELOCITY (Km/s)	ENERGY (eV)
⊙	159	HELIUM	O_2^+	10.8	19.0
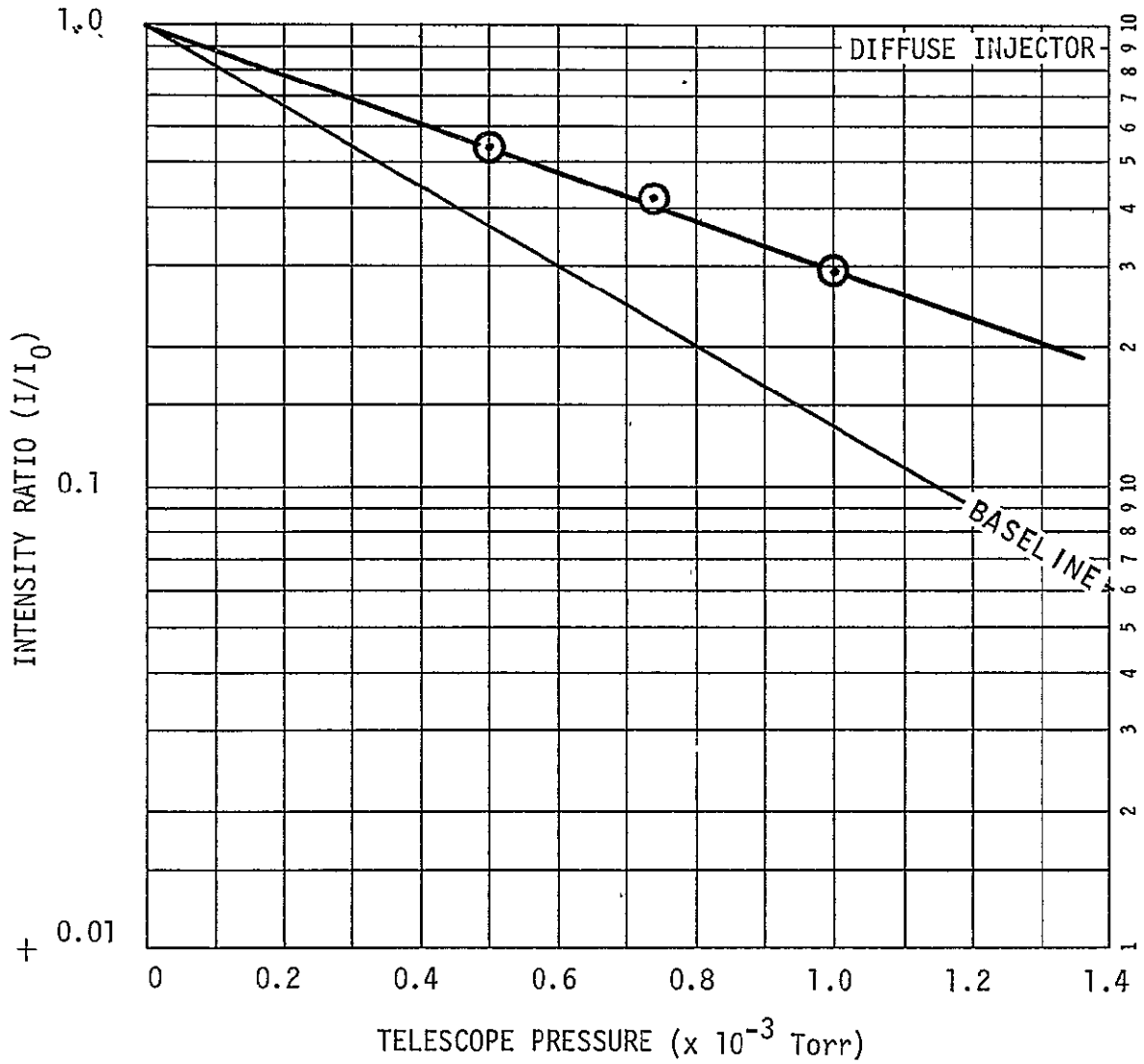
Figure 4-8 O_2^+ Attenuation Versus Pressure

4-11
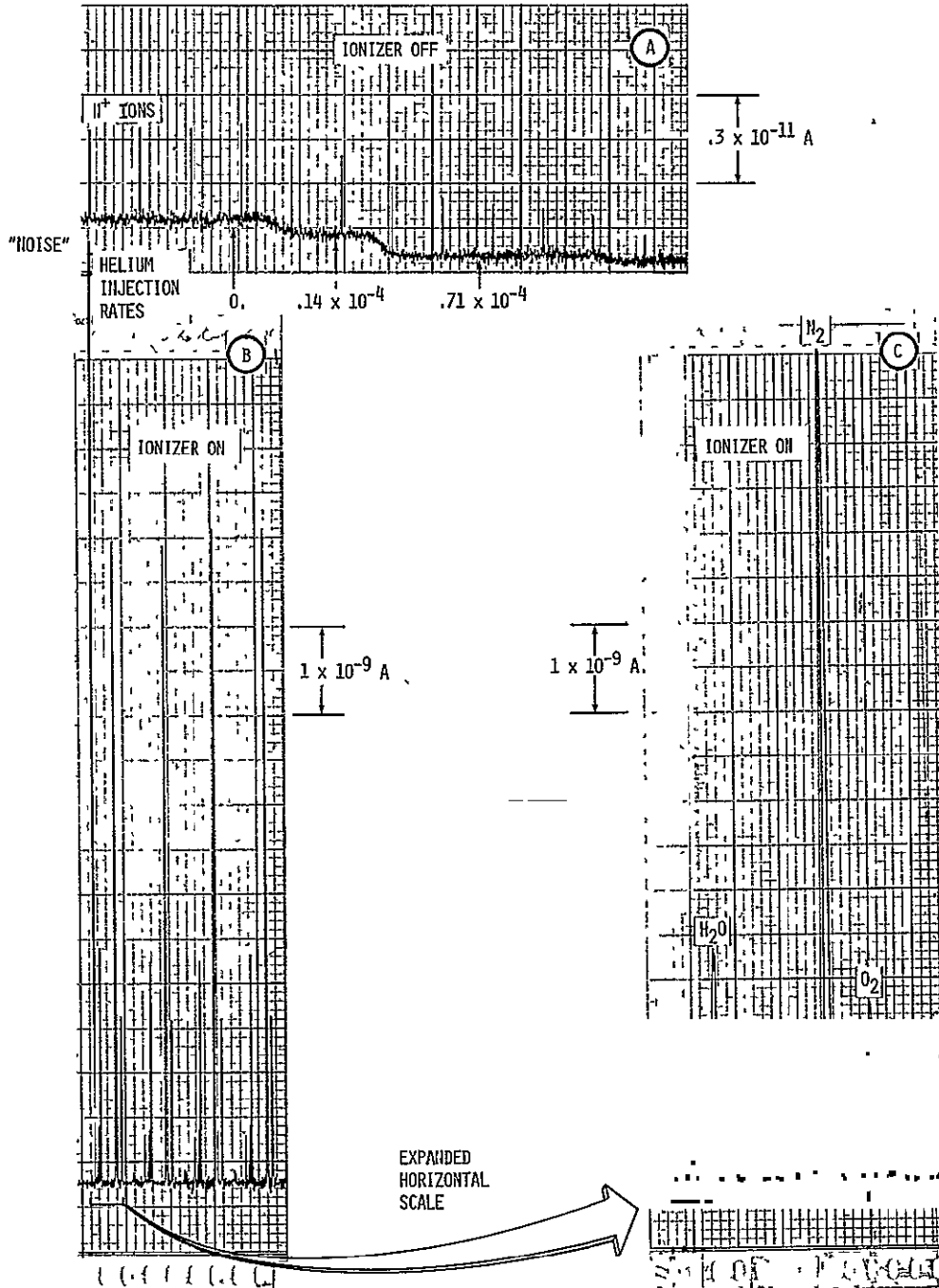
Figure 4-9 Mass Spectrometer Output with N$^+$ Ion Beam

4-12

peaks with the ionizer off, a scan was made with the ionizer activated on a less sensitive scale. It was noted that in addition to N, background gases H_2O, O_2 and N_2 were observed. When N_2 is ionized by the RGA a portion is normally dissociated in N as well. Table 4-I which illustrates typical fracture patterns for H_2O, O_2 and N_2 shows that the N peak is expected to be 6.% of the N_2 peak. To bring the N^+ ion peaks from the ion gun shown in Ⓐ out of the noise level created by fracturing N_2, the background gases would have to be reduced by a factor of 300 to 1000. This would require a background pressure on the order of 10^{-8} for N_2. It was hoped that if N^+ or O^+ ions from the ion source could be distinguished from fractured residual gases, H_2O could be bled into the chamber and used as a charge-exchange mechanism.

The "noise" level on the signal from the electron multiplier may be high energy neutrals that can pass through the quadrupole selector undeflected and activate the electron multiplier.

Based on earlier suggestions by NASA Ames personnel, H_2O^+ ions were injected into the telescope and N_2 gas was used as the scattering medium. When the telescope was cooled to LN_2 temperatures the residual water vapor in the chamber was lowered but the background levels of H_2O were still comparable to the signal generated by the H_2O^+ ions from the ion source. Additional cryopanels around the chamber walls would probably lower the background H_2O levels to within acceptable limits.

In conclusion, the attempts to identify high velocity neutrals were not successful with the existing test configuration.

Table 4-1   Normalized Cracking Patterns for Spectrascan 750

AMU					Parent				
	CH_4	H_2O	N_2	CO	C_2H_6	O_2	Ar	CH_3OH	CO_2
12	1.5			1.8	0.3				4.8
13	5.7				0.7				
14	12.6		6.0	2.0	2.3				
15	77.6				3.9				
16	100%	2.1		0.77	0.1	21.1			11.1
17		24.3						0.4	
18		100%						1.7	
19									
20							10.5		
24					0.5				
25					3.5				
26					22.6				
27					32				
28			100%	100%	100%			6.7	18.1
29				0.64	19.7			63.4	
30				0.1	25.6			1.0	
31					0.6			100%	
32						100%		65.5	
36									
37									
38									
39									
40							100%		
41									
42									
43									
44									100%

Peak heights are expressed as a percentage of the highest peak.
Partial Pressure of Parent 1×10^{-5} Torr   Ionizing Current   1 ma
Ionizing Voltage   70 volts   Resolution M/ ΔM 100@M = 50

5.0 CONCLUSIONS

5.0 CONCLUSIONS

The following conclusions can be drawn as a result of the analysis and laboratory testing that was conducted during this study.

- Within the limitations of this simulation of on-orbit conditions, it was demonstrated that a helium purge system can be an effective method of reducing the incoming flux of contaminant species.

- A helium purge system would appear to be a feasible technique for reducing deposition of condensibles on cryogenic surfaces and for extending the operational lifetime of the SIRTF.

- Based on the subscale results, a 90% reduction in O, N_2, and H_2O at the primary optics of the SIRTF can be obtained using 20K helium with a pressure of 1×10^{-5} Torr and a flow rate of less than 0.1 g/s.

- Although a generalized purge.system was employed in conjunction with basic telescope components, the simulation provided data that can be used for further modeling and design of a specific helium injection system.

- Experimental telescope pressures required for 90% attenuation appears to be slightly higher (factor of 2 to 5) than predicted by Murakami (1).

- Cooling the helium purge gas and telescope components from 300K to 140K had no measurable effect on the stopping efficiency of a given mass flow of helium from the diffuse injector.

- The use of a 25 degree half-angle nozzle to inject the helium was slightly less effective than a porous plug (diffuse injector).

- Continuum gas dynamic computer programs were used to design the small low density hypersonic nozzle. Because these

programs are not normally used to evaluate low operating
pressures and temperature, the optimum nozzle may not
have been used.

- O^+ and H_2O^+ ions exhibit nearly the same attenuation while N_2^+ was attenuated more for the same helium purge conditions.

- Changing the magnitude of the flux levels of N_2^+ by a factor of 10 while maintaining a constant velocity, showed no measurable differences in the normalized attenuation, I/I_o.

- Residual gases within the chamber thwarted two preliminary attempts to observe high energy neutrals formed by charge-exchange interactions.

- Air appeared to be a more efficient stopping medium than helium but charge-exchange interactions may have neutralized the N_2^+ ion beam and complicated the data interpretation.

6.0 RECOMMENDATIONS

6.0 RECOMMENDATIONS

The present study has shown the feasibility of using a helium gas purge to minimize the low earth orbit ambient environment contaminants for an infrared telescope such as the SIRTF. However, before an effective full scale helium purge system can be designed, a more comprehensive set of test data should be acquired. This comprehensive data base would provide the basis to set the requirements for the design of such a system. The following recommendations are made to support the development of such a data base.

a) Conduct a parametric experimental study to acquire the technical data base needed to support the helium purge design. The parametric study would encompass:

1) other contaminant species with additional effort on neutral detection,

2) an extended energy range (particularly on the low energy end) to understand velocity dependence,

3) several helium injection configurations and locations,

4) lower temperatures for the purge gas,

5) other types of purge gas (e.g. argon or neon),

6) off axis measurements where the telescope axis is not parallel to the direction of the incoming flux,

7) actual collision cross section measurements with consideration given to inelastic collisions such as charge-exchange and excitation of internal energy modes and

8) a simulation of on-orbit return flux.

b) Incorporate the following improvements to the existing experimental setup:

1) modify the ion gun to enhance low energy ion flux levels,

2) develop a neutral beam of contaminants,

3) improve the scale model geometry by including SIRTF structural elements such as baffles and secondary optics structure,

4) include additional cryogenic panels in the chamber to minimize residual gases,

5) incorporate true pressure measurements to verify telescope conditions at low temperatures, and

6) improve helium gas and telescope cooling technique.

c) Perform a parallel analytical effort to review the applicability of current theoretical calculations and establish the appropriate scaling laws which can be used with the date base to design a helium purge system.

d) Explore some of the anomalies observed during the test, for example:

1) normally a positive current was collected on the end plate of the telescope due to the impingement of positive ions. During several runs a negative current was observed on the barrel section of the telescope that appeared to be associated with the flow of helium.

2) the gain of the electron multiplier on the RGA would deteriorate after an hour or more of continuous testing with the ion beam as if the detector was being poisoned.

3) a small background current (5-10% of primary beam) was observed on the telescope end plate and RGA detector that was unaffected by the velocity filter. This current appeared to be a function of the ionizing voltage used within the ion gun.

7.0 ACKNOWLEDGEMENTS

7.0 ACKNOWLEDGEMENTS

8.0 REFERENCES

8.0 REFERENCES

1) Murakami, N.: "Theoretical Contamination of Cryogenic Satellite Telescopes," NASA TP - "Final Proof Copy", Ames Research Center, October, 1977.

2) Witteborn, F. C. and Young, L. S.: "Spacelab Infrared Telescope Facility (SIRTF)," J. Spacecraft, Vol. 13, No. 11, November, 1976, pp. 667-674.

3) Simpson, J. P. and Witteborn, F. C.: "The Effect of the Shuttle Contaminant Environment on a Sensitive Infrared Telescope," Applied Optics, Vol. 16, No. 8, August 1977.

4) "Shuttle Infrared Telescope Facility (SIRTF) Preliminary Design Study - Final Report," Data Item I.D.-9, Hughes Aircraft Company, Electro-Optical Division, August 1976.

5) Wahlin, L.: "The Colutron, A Zero Deflection Isotope Separator," Nuclear Instruments and Methods, Vol. 27, No. 1, 1964.

6) "Digital Computer Programs for Rocket Nozzle Design and Analysis," Pratt & Whitney Aircraft Report PWA FR-1021, 26 June 1964.

7) Curry, D. M. and Stephens, E. W.: "Boundary Layer Integral Matrix Procedure - User's Manual," Version C NAS9-9494.

8) Dushman, S.: "Scientific Foundation of Vacuum Technique," Wiley & Sons, Inc., October 1960, pg. 193.

9) Johnson, F. S.: "Satellite Environment Handbook," Stanford University Press, 1961.

10) Bates, D. R.: "Atomic and Molecular Processes," Academic Press, New York, 1962, pg. 669.

11) Simons, J. H., Muschlitz, E. E. and Unger, L. G.: J. Chem Phys., Vol. 11, 1943, pg. 322.

APPENDIX A

LIST OF INSTRUMENTATION

LIST OF INSTRUMENTATION USED DURING HELIUM PURGE STUDY

Instrument	Part #	Location
RGA–Granville Phillips Spectroscan 750 Mass Spectrometer	EQ52615	End of telescope
Veeco Thermocouple Gauge	590382	He inlet to telescope
Ionization Gauge	590382	Telescope
Veeco Thermocouple Gauge	590383	Vacuum chamber
Ionization Gauge	590383	Vacuum chamber
HP 7100B Strip Chart Recorder	531488	All thermocouples
HP 7100B Strip Chart Recorder	534411	RGA
Tektronix Type 556 Dual Beam Oscilloscope	527673	RGA
Hastings Model: CVH–3 Vacuum Gauge	39	Gas inlet on ion gun
Hastings Model: CVH–3 Vacuum Gauge	40	Density Gauge
Kepco Model: PR 155–4M Regulated D.C. Supply	056121	Ion gun
Regation Semiconductor Power Supply	AF031972	Ion gun
Keithley electrometer Model 610A	590026	
Colutron Velocity Filter		Ion gun
Fluke 415B High Voltage Power Supply	526774	Ion gun (ion acceleration)
HP 5264B DC Power Supply	S36359	Velocity filter (magnet supply)
Fluke Model 5 Power Supply	590032	Velocity filter (Electric field supply)
Fischer Porter Flow Meter		Helium Flow System

A-1

APPENDIX B

DRAWINGS OF TELESCOPE ASSEMBLY
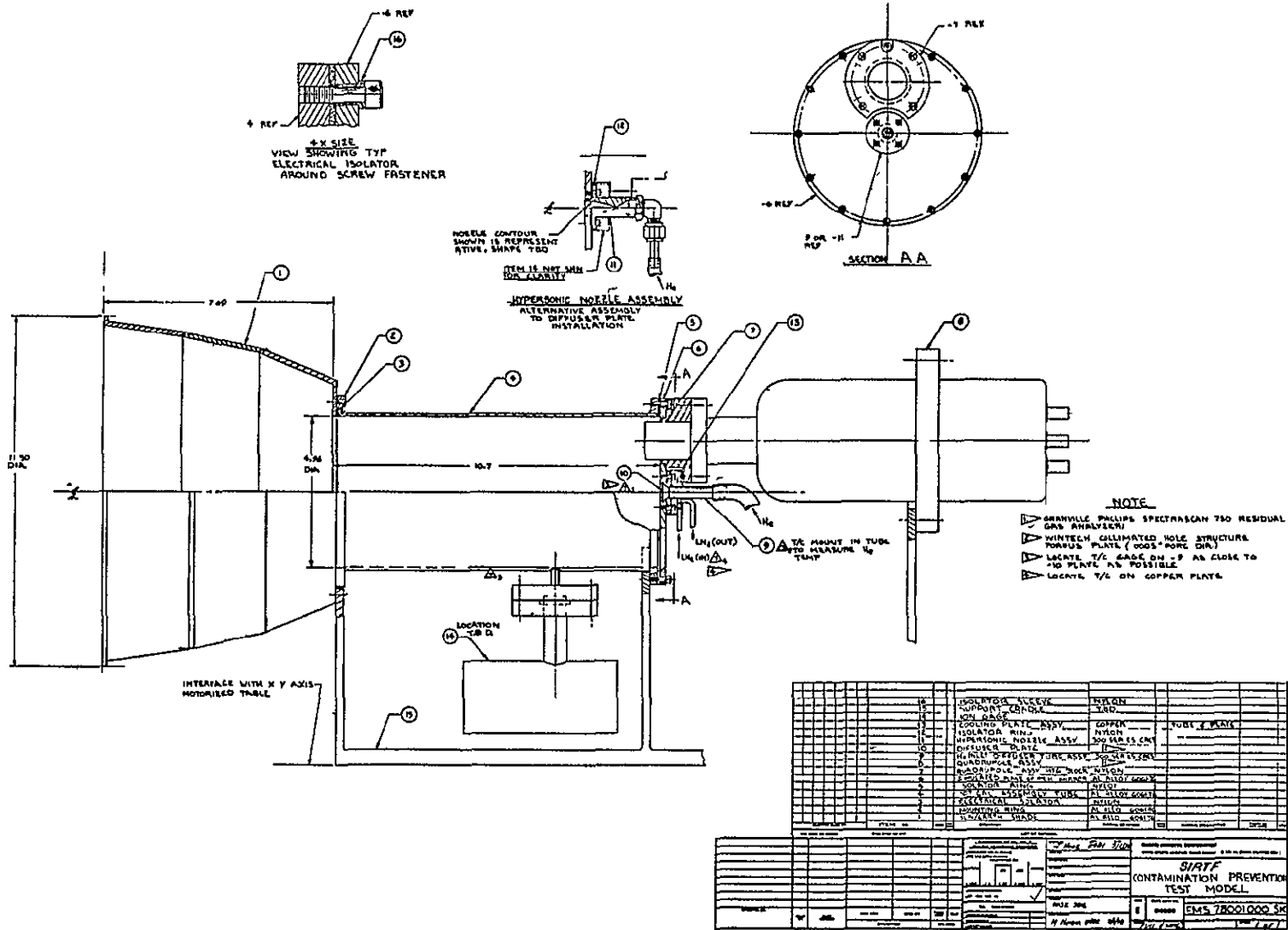
Figure B-1 Engineering Drawing of Overall Telescope Design and Related Instrumentation

Figure B-2 Sunshade Design Dimensions

Figure B-3   Telescope Housing and Flange Dimensions

APPENDIX C

TYPICAL OUTPUT FROM NOZZLE DESIGN CODE

BELL NOZZLE DESIGN

SAMPLE CASE   GAMMA = 1.666

PERFECT GAS,
AXISYMMETRIC FLOW

THE INPUT IS --

N =	0	N1 =	20	NE =	40
NSL =	0	NA =	1	K2 =	0
FCON =	1.0000000	R =	0 0000000	GAMMA =	1.6660000
PITOL =	.0050000	DELX =	.1000000	PC =	0.0000
CYLHT =	.010000	PA =	0.000000	FM =	1.005000
YT =	1.000000	ATOL =	.005000		
CF1 =	.003000	FROZEN =	0.000000		

THE FIRST MACH LINE IS

X	Y	TANGENT THETA	VELOCITY	TANGENT ALPHA	MASS FLOW
0	1.0000000E+00	0.	5.0168367E-01	9.9875234E+00	1.6229040E-01
5.2170354E-03	9.4789474E-01	0	5.0168367E-01	9.9875234E+00	1.4581700E-01
1.0434071E-02	8.9578947E-01	0.	5.0168367E-01	9.9875234E+00	1.3022491E-01
1.5651106E-02	8.4368421E-01	0.	5.0168367E-01	9.9875234E+00	1.1551413E-01
2.0868142E-02	7.9157895E-01	0	5.0168367E-01	9.9875234E+00	1.0168466E-01
2 6085177E-02	7 3947368E-01	0.	5 0168367E-01	9.9875234E+00	8.8736499E-02
3.1302212E-02	6.8736842E-01	0	5 0168367E-01	9.9875234E+00	7.6669653E-02
3.6519248E-02	6.3526316E-01	0.	5 0168367E-01	9.9875234E+00	6.5484118E-02
4.1736283E-02	5.8315789E-01	0.	5.0168367E-01	9.9875234E+00	5.5179894E-02
4.6953319E-02	5.3105263E-01	0.	5.0168367E-01	9.9875234E+00	4.5756993E-02
5.2170354E-02	4.7894737E-01	0.	5 0168367E-01	9.9875234E+00	3.7215383E-02
5.7387389E-02	4.2684211E-01	0.	5.0168367E-01	9.9875234E+00	2.9555094E-02
6.2604425E-02	3.7473684E-01	0.	5.0168367E-01	9.9875234E+00	2 2776117E-02
6.7821460E-02	3 2263158E-01	0.	5.0168367E-01	9.9875234E+00	1.6878451E-02
7.3038496E-02	2.7052632E-01	0.	5.0168367E-01	9.9875234E+00	1.1862097E-02
7.8255531E-02	2.1842105E-01	0.	5.0168367E-01	9.9875234E+00	7.7270547E-03
8.3472567E-02	1.6631579E-01	0.	5.0168367E-01	9.9875234E+00	4.4733237E-03
8.8689602E-02	1.1421053E-01	0.	5.0168367E-01	9.9875234E+00	2.1009043E-03
9.3906637E-02	6.2105263E-02	0.	5.0168367E-01	9.9875234E+00	6.0979637E-04
9.9123673E-02	1.0000000E-02	0.	5.0168367E-01	9.9875234E+00	0.

THIS NOZZLE IS DESIGNED FOR A/A* = 100.00000

X/R	Y/R	TANGENT THETA	M	P/PC	GAMMA	AE/AT	AS/AT	CTG	CTN
0.0000	1.0000	.35822	1.90440	.13792	1.66600	1.0001	0.000	1.29897	1.28797
.0971	1.0815	.39839	2.05372	.11139	1.66600	1.1699	.264	1.32005	1.30889
.5183	1.2668	.43751	2.31778	.07687	1.66600	1.6050	1.345	1.35971	1.34792
1.1010	1.5387	.43489	2.65044	.04899	1.66600	2.3678	3.149	1.40604	1.39345
1.8391	1.8619	.39776	3.05224	.02928	1.66600	3.4672	5.889	1.44772	1.43427
2.7214	2.2156	.36109	3.44146	.01836	1.66600	4.9095	9.765	1.48083	1.46648
3.7456	2.5877	.32744	3.81515	.01207	1 66600	6 6969	15.001	1.50726	1.49200
4.8988	2.9701	.29705	4.17555	.00825	1.66600	8.8227	21.754	1.52838	1.51223
6.1866	3 3580	.26952	4.52680	00582	1.66600	11.2776	30.266	1.54535	1.52833
7.6116	3 7476	.24455	4.87085	.00422	1.66600	14 0460	40.764	1.55905	1.54118
9.1713	4.1361	.22194	5.20896	.00312	1.66600	17.1091	53.437	1.57015	1.55148
10.8773	4.5211	.20134	5.54233	.00236	1.66600	20 4429	68.580	1.57920	1.55974
12.7305	4.9008	.18257	5.87145	.00181	1.66600	24.0207	86.405	1.58659	1.56638
14.7330	5.2735	.16544	6.19642	.00141	1.66600	27.8130	107.132	1.59265	1.57172
16.8981	5.6372	.14957	6.51992	.00111	1.66600	31.7823	131.028	1.59763	1.57600
19.2295	5.9905	.13505	6.83882	.00089	1.66600	35.8906	158.510	1.60172	1.57943
21.7315	6.3319	.12160	7.15539	.00072	1.66600	40 0974	189 630	1.60509	1.58216
24.4147	6.6596	.10898	7.47212	.00059	1.66600	44 3555	224.753	1.60785	1.58432
27.2519	6.9745	.10152	7.69587	.00051	1.66600	48.6488	263.677	1.61019	1.58605
30.1905	7.2805	.09184	7.97273	.00043	1.66600	53.0121	305 798	1.61224	1.58753
33.3306	7.5697	.08226	8.25712	.00036	1.66600	57.3064	352.632	1.61394	1.58867
36.6482	7.8425	.07350	8.53226	.00031	1.66600	61.5119	403.942	1.61535	1.58955
40.1405	8.0985	.06543	8.73865	.00027	1.66600	65.5933	459.769	1.61653	1.59021
43.8129	8.3366	.05796	9.05689	.00023	1.66600	69.5067	520 259	1.61751	1.59069
47.6625	8.5564	.05099	9.30770	.00020	1.66600	73 2204	585.403	1.61832	1.59102
51.7177	8.7551	.04512	9.53097	.00018	1.66600	76 6614	655.697	1.61899	1.59120
55.8361	8.9459	.04140	9.68980	.00017	1.66600	80 0379	728.684	1.61958	1.59133
60.1309	9 1177	.03574	9.91330	.00015	1.66600	83 1431	806.335	1.62007	1.59137
64.5852	9.2716	.03084	10.11464	.00014	1.66600	85.9735	888.305	1.62048	1.59134
69.1923	9.4080	.02636	10.30395	.00012	1.66600	88 5208	974.413	1.62081	1.59124
73.9483	9.5270	.02223	10.48215	.00011	1.66600	90.7745	1064.506	1.62108	1.59109
78.8768	9.6268	.01838	10.65106	.00011	1.66600	92.6860	1158.937	1 62129	1.59089
83.8879	9.7137	.01500	10.80204	.00010	1.66600	94.3673	1255.878	1.62147	1.59066
88.9840	9.7907	.01296	10.90004	.00009	1.66600	95 8701	1355.298	1.62161	1.59041
94.2142	9.8521	.01015	11.02853	.00009	1.66600	97.0757	1458.053	1.62172	1.59013
99.5489	9.9004	.00766	11.14282	.00009	1.66600	98.0287	1563.444	1.62181	1.58983
104.9803	9.9364	.00543	11.24580	.00008	1.66600	98.7433	1671.200	1.62187	1.58951
110.4980	9.9614	.00352	11.33426	.00008	1.66600	99.2404	1781.005	1.62190	1.58918
116.0922	9.9765	.00186	11.41096	.00008	1.66600	99.5425	1892.555	1.62193	1.58883
121.7496	9.9834	.00076	11.46127	.00007	1.66600	99.6810	2005.490	1.62194	1.58847
127.5777	9.9838	0.00000	11.51006	.00007	1.66600	99.6877	2121.875	1.62194	1.58810

APPENDIX D

SAMPLE INPUT FOR BLIMPK CODE

```
10100420z 0202000000 SIRTF HELIUM PURGE NOZZLE BOUNDARY LAYER EVALUATION
             IDENT
02 NELM
01 NCAS
-1.
08 NSTA
 0.00001   .0001314   .000733   .0015972   .0057208   .0119413   .020570   .04059
13 NETA
      .000       .024      .040       .072       .120       .200      .320      .480
      .800      1.400     2.000      3.200      5.000
11    .9500
 .00100   .0011213   .0014137   .001820   .003361   .005044   .0067183   .00929
      .0010    PRESSURE
      223.2    STAG ENTHALPY
      0 000
      .4400     11.823     .0180      .9000      .9000      250.
      223.2 GW  WALL GUESS
003  .4310      23.40      32.00      3.467      106.7 ,    .4340     24.30     50000.
     2HELIUM      4.0026    -.99930 0.0       0.0        0 0       0.0       0.0       0.0
     1HYDROGEN    1.00797   -.00001 0.0       0.0        0.0       0.0       0.0       0.0
     99ELECTRON   0.0005490.0        0.0       0.0        0.0       0.0       0.0       0.0
     2  1  0  0  0  0  0  0  0  0  0  0  0 OSTP - 06/71              H2
     000000+0 238063+5 750300+1 320359-3-852519+4 486337+2   10.10000.1   0.H2
     000000+0 233362+5 894087+1 141828-3-631695+7 484712+210000.25000.1   0.H2
     1  2  0  0  0  0  0  0  0  0  0  0  0 OSTP - 06/71              HE
     000000+0 149038+5 496792+1 000000+0 000000+0 415942+2   10.10000.1   0.HE
     000000+0-502948+5-213509+1 332810-3 427616+9 261981+210000.25000.1   0.HE
     1  1  0  0  0  0  0  0  0  0  0  0  0 OSTP - 06/71              H
     531012+5 134180+5 496507+1 868933-6 390850+2 388601+2   10.10000.1   0.H
     531012+5-148656+6-194223+2 134546-2 1.1640+9-385316-110000.25000.1   0.H
     1 99  0  0  0  0  0  0  0  0  0  0  0 OSTP - 06/71              E-
     000000+0 149038+5 496792+1 000000+0 000000+0 164597+2   10.10000.1   0.E-
     000000+0 149038+5 496792+1 000000+0 000000+0 164597+210000.25000.1   0.E-

 .12829   .09785    .06144    .03056    .00573    .00174    .00068    .00021
      IPRE
 0.
 0.
      180.      180.      180.      180.      180.      180.      180.      180.
      ITW
 0.
 0.
 0.
 0.
 0.
 0.
      IFLUXU
```

APPENDIX E

DISCUSSION OF IONIZATION GAUGE OUTPUT

An ionization gage was used to monitor the pressure in the
scale model telescope and in the probe used to map the helium
plume. In actuality, this instrument did not measure pressure as
used in the context of the perfect gas law. Pressure, as used in
vacuum technology, has other interpretations than its definition
in gas kinetic theory as a force per unit area or momentum flux
on a surface. Many of the so called methods of pressure measure-
ment are actually measurements of some related gas property.
When gage readings are discussed in the preceding text in terms
of pressure, it should be noted that the term is being used in its
imprecise sense.

Ionization gages are characterized by a sensing zone located
in an enclosing envelope which in turn communicates with the
vacuum space to be measured. The gage ionizes the gas within the
glass enclosure with electrons obtained from a heated filament.
For a specific electron emission current, the ion current reach-
ing the collector is taken as a measure of pressure. The gage
used on the telescope was the inverted Bayard-Alpert type shown in
Figure E-1. The central electrode is the ion collector which
operates at ground potential, while the filament is maintained at
25 to 50 volts above ground potential, and is heated to produce
electron emission at a desired current level, often about 10
milliamperes. The electrons so produced are accelerated through
an additional potential of about 150 volts. Subsequently, the
electrons are collected on the electron collector which is usually
called the grid.

The gas entering the gage will be modified by collisions
with the glass envelope which may adsorb part of it, add desorbed
material, or change the temperature of the gas. Further modifica-
tions occur by collisions with the electron emission current designed to
ionize the gas. In the process, information regarding its initial
state prior to entering the gage is erased.

Generally, the ionization gage should be regarded as a means
of measuring the incident flux density of molecules entering the
gage aperture. The temperature of the gage enclosure affects
the concentration and pressure within the gage but does not affect
the flux density entering the glass envelope. It was observed
that the telescope "pressure" (measured by the ionization gage)

— ION COLLECTOR, GROUND POTENTIAL

—"GRID",ELECTRON COLLECTOR
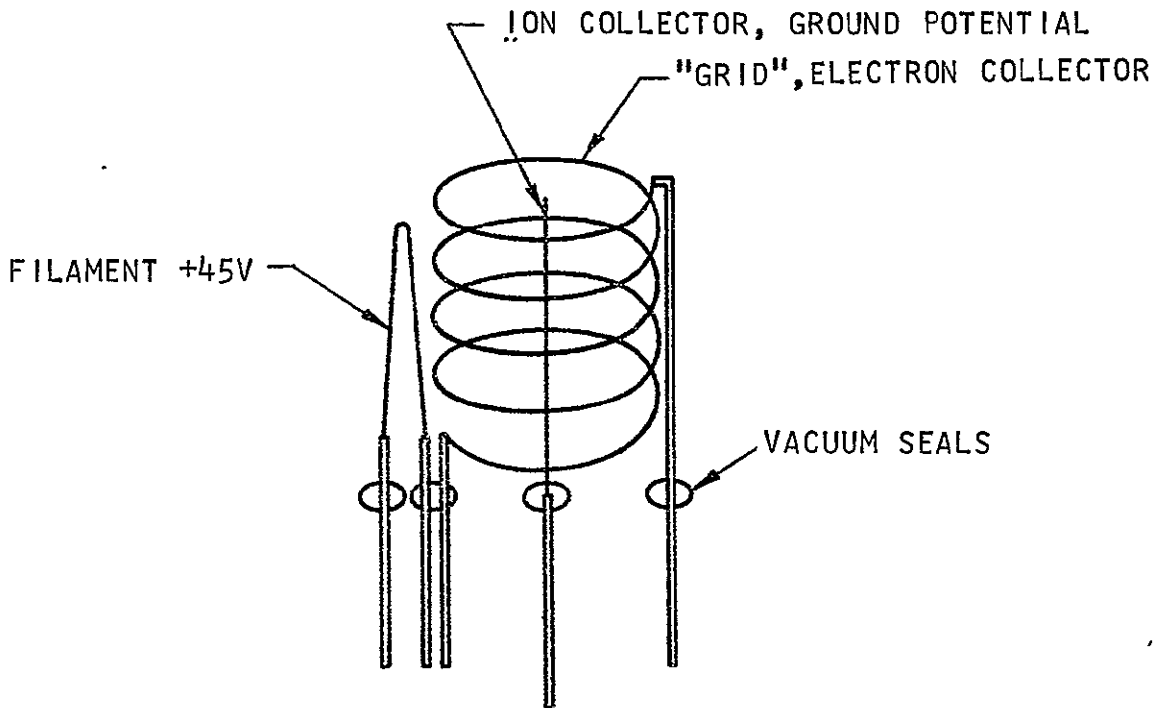
FILAMENT +45V —

VACUUM SEALS

Figure E-1.   Sketch of an Inverted Bayard-Alpert Type Ionization
Gage Used to Measure the Telescope "Pressure"

for a given mass flow of helium did not change when the helium
temperature was lowered by a factor of two. Rather than measure
pressure as intended, the gage simply verified that the mass flux
thru the telescope (and to the entrance to the gage) was the same
for the 300K and 140K gas flows. Dushman (8) discusses other
"pressure" measuring devices such as the Knudsen gage which does
operate on a momentum principle. It appears however that these
other devices are not tools but more like experiments in themselves.

The response of the ionization gage is a function of the
chemical species being measured. The relative sensitivities
for gases observed in this test are shown in the table below.
Only the nitrogen and helium values were actually calibrated for
this test.

Table E-1   Ionization-Gage Sensitivity Relative to Nitrogen for
Various Gases (Taken from Sentaler)[*]

Gas type	Sensitivity Factor
Nitrogen	1.0 (calibrated)
Oxygen	0.8
Hydrogen	.4-.5
Carbon dioxide	1.3-1.6
Water vapor	1.1-2,0
Argon	1.2-1.5
Neon	.25-.32
Helium	.18(calibrated)

The following procedure was used to convert the raw data read from the ionization gage controller to a pressure.

Prior to injecting helium, a background reading, B, was taken of the residual gases in the chamber. Analysis of these gases with the mass spectrometer indicated the predominant species were N_2, O_2 and H_2O. The reading was then transferred to the calibration curve developed for the instrument at the Denver Division's Metrology Laboratory for N_2 which resulted in a calibrated value, B_c.

The helium flow was then initiated and a new reading was obtained from the output of the gage controller, A. This was then adjusted to A_c with the calibration curve. The difference between A_c and B_c is the result of helium. According to the helium calibration, this must be increased by a factor of 5.43 to reflect the different ionization potential of helium. The procedure is summarized by the following equation:

$$P = (A_c - B_c) \times 5.43 + B_c.$$

---

[*] Santeler et.al.: Vacuum Technology and Space Simulation, NASA SP-105